THE JOURNAL OF COMPARATIVE NEUROLOGY 505:493–510 (2007)

Morphology and Ontogeny of Rat Perirhinal Cortical Neurons

SHARON CHRISTINE FURTAK,[1] JAMES RUSSELL MOYER JR,[2] AND THOMAS HUNTINGTON BROWN[1,3]*
[1]Department of Psychology, Yale University, New Haven, Connecticut 06520
[2]Department of Psychology, University of Wisconsin-Milwaukee, Milwaukee, Wisconsin 53201
[3]Department of Cellular and Molecular Physiology, Yale University, New Haven, Connecticut 06520

ABSTRACT

Golgi-impregnated neurons from rat perirhinal cortex (PR) were classified into one of 15 distinct morphological categories (N = 6,891). The frequency of neurons in each cell class was determined as a function of the layer of PR and the age of the animal, which ranged from postnatal day 0 (P0) to young adulthood (P45). The developmental appearance of Golgi-impregnated neurons conformed to the expected "inside-out" pattern of development, meaning that cells populated in deep before superficial layers of PR. The relative frequencies of different cell types changed during the first 2 weeks of postnatal development. The largest cells, which were pyramidal and spiny multipolar neurons, appeared earliest. Aspiny stellate neurons were the last to appear. The total number of Golgi-impregnated neurons peaked at P10–12, corresponding to the time of eye-opening. This early increase in the number of impregnated neurons parallels observations in other cortical areas. The relative frequency of the 15 cell types remained constant between P14 to P45. The proportion of pyramidal neurons in PR (≈50%) was much smaller than is typical of neocortex (≈70%). A correspondingly larger proportion of PR neurons were nonpyramidal cells that are less common in neocortex. The relative frequency distribution of cell types creates an overall impression of considerable morphological diversity, which is arguably related to the particular manner in which this periallocortical brain region processes and stores information. J. Comp. Neurol. 505:493–510, 2007.

Indexing terms: medial temporal lobe; development; Golgi-Cox; laminar distribution; periallocortex; pyramidal; nonpyramidal

The perirhinal cortex (PR) is a medial temporal lobe structure that has been implicated in aspects of both perception and memory (Meunier et al., 1993; Zola-Morgan et al., 1993; Buckley and Gaffan, 1998a,b; Liu and Bilkey, 1998, 2001; Bucci et al., 2000, 2002; Bussey et al., 2000, 2002, 2003; Holdstock et al., 2000; Buckley et al., 2001; Eacott and Norman, 2004; Hannesson et al., 2004; Lindquist et al., 2004; Norman and Eacott, 2004; Lee et al., 2005). Damage to this and surrounding areas of the parahippocampal region result in severe memory loss and amnesia (Scoville and Milner, 1957; Zola-Morgan et al., 1989; Suzuki et al., 1993; Buffalo et al., 1998; Levy et al., 2004). It is worth noting in this respect that Alzheimer's disease (AD), a well-known cause of amnesia, preferentially targets PR and the anatomically adjacent entorhinal cortex (EC). More specifically, PR and EC are the first cortical areas to show neurodegeneration associated with AD (Van Hoesen et al., 2000). Furthermore, as AD progresses into late stages PR continues to be one of the most affected cortical regions (Arnold et al., 1991; Braak and Braak, 1991, 1995; Van Hoesen and Solodkin, 1994; Juottonen et al., 1998; Van Hoesen et al., 2000). Our interest in the cellular neurobiology of PR stems partly

Grant sponsor: National Institute on Aging (NIA); Grant number: AG019645; Grant sponsor: National Institute of Mental Health (NIMH); Grant number: MH58405 (to T.H.B.).

*Correspondence to: Thomas H. Brown, 2 Hillhouse Ave., Rm. 106, Dept. of Psychology, Yale University, New Haven, CT 06520.
E-mail: thomas.brown@yale.edu

Received 18 January 2006; Revised 13 April 2007; Accepted 23 August 2007

DOI 10.1002/cne.21516

Published online in Wiley InterScience (www.interscience.wiley.com).

from an attempt to better appreciate its functional contributions to perception and memory as well as from a desire to understand the reason for the selective vulnerability of this brain region to neurodegeneration.

In the rat, PR is composed of two adjacent strips of cortex spanning the ventral and dorsal banks of the caudal section of the rhinal sulcus (Brodmann's areas 35 and 36, respectively). This periallocortical region contains remarkably low amounts of myelin (Burwell, 2001; Brown and Furtak, 2006), consistent with the unusually low conduction velocities in PR axons (Moyer et al., 2002). Perirhinal cortex receives unimodal inputs from all sensory modalities as well as polymodal inputs from association areas (Burwell and Amaral, 1998a,b; Burwell, 2000; Furtak et al., 2007). There are extensive reciprocal connections between PR and EC, hippocampus, and the amygdala (Romanski and LeDoux, 1993; Burwell and Amaral, 1998a,b; Naber et al., 1999; Shi and Cassell, 1999; Burwell, 2000; Pitkänen et al., 2000; Pikkarainen and Pitkänen, 2001; Furtak et al., 2007). Based on its connectivity, PR appears to be well positioned to control information flow to and from these mnemonically important structures.

Understanding the distinctive characteristics of PR neurons and their organization could be an important first step in elucidating the causes behind the selective vulnerability of these neurons to neurodegeneration in AD. This same knowledge is also necessary for grasping how PR neurons and circuits process and store information. Recent studies of rodents have greatly advanced our knowledge of the architecture, connectivity, and neurophysiology of PR (Bilkey, 1996; Liu and Bilkey, 1996; Burwell and Amaral, 1998a,b; Faulkner and Brown, 1999; Naber et al., 1999; Shi and Cassell, 1999; Beggs et al., 2000; Burwell, 2000, 2001; Pitkänen et al., 2000; Cho et al., 2001; D'Antuono et al., 2001; McGann et al., 2001; Pikkarainen and Pitkänen, 2001; Moyer et al., 2002; Allen et al., 2007; Furtak et al., 2007). However, the morphology of PR neurons has received relatively little attention, in contrast to neocortex and allocortex. In particular, there have been no detailed Golgi studies of PR neuronal morphology. Recall that PR is classified as periallocortex, a phylogenic "transition" from allocortex to neocortex. The classical Golgi studies by Ramón y Cajal (1911) and Lorente de No (1933, 1934) supplied the first insights into neuronal morphology in cerebral cortex, but devoted little attention to PR.

The only information about the distribution of morphological cell types in rat PR comes from reconstructions of 217 biocytin-filled neurons. All of these neurons were characterized neurophysiologically using whole-cell recordings (WCRs) from horizontal brain slices (Moyer and Brown, 1998, 2007; Faulkner and Brown, 1999; McGann et al., 2001; Moyer et al., 2002). The considerable morphological diversity that was apparent in this small sample suggested that a much larger sample would be needed to appreciate the distribution and development of cell types in PR. For sampling cellular neuroanatomy, the Golgi technique has historically been the standard against which other methods are compared. Although the mechanism by which neurons are selected for impregnation still remains a mystery, the best estimate is that the Golgi-Cox method randomly impregnates ≈1–2% of the neurons when compared to Nissl counterstains (Smit and Colon, 1969; Pasternak and Woolsey, 1975). The present study uses a modified Golgi-Cox method to investigate rat PR morphology and development. This approach circumvents biases that may exist in the published samples of biocytin-labeled PR neurons, which were visually selected for WCRs. Here we describe the laminar distribution and ontogeny of 15 morphological types in a sample of 6,891 PR neurons.

Abbreviations

AD	Alzheimer's disease
BLA	Basolateral nuclear complex of the amygdala
CP	Cortical plate
dH_2O	Deionized water
ec	External capsule
EC	Entorhinal cortex
i.p.	Intraperiotoneal
IZ	Intermediate zone
LA	Lateral nucleus of the amygdala
MZ	Marginal zone
NA	Numerical aperture
P	Postnatal day
PR	Perirhinal cortex
WCRs	Whole-cell recordings

MATERIALS AND METHODS

Animals

Fifty-seven male Sprague-Dawley rats (Charles-River Laboratories, Wilmington, MA) were sacrificed at different postnatal ages (postnatal day 0, P0, through P45). Of these, a total of 20 animals were used for morphological classification during development (n = 2 animals per age group). The exact ages in each age group were as follows: 0 day group (P0; P0), 1 day group (P1; P1), 4–5 day group (P4; P5), 6–9 day group (P6; P8), 10–12 day group (P10; P12), 14–17 day group (P14; P17), 18–22 day group (P18; P22), 28–32 day group (P28; P31), 35–40 day group (P36; P40), 42–45 day group (P44; P45). A total of 38 animals were used for two- and three-dimensional reconstructions of neurons, 17 of which were also used for morphological classifications. Their exact ages were: P4 (n = 2); P5 (n = 2); P6 (n = 2); P8 (n = 1); P9 (n = 1); P10 (n = 1); P11 (n = 1); P12 (n = 2); P14 (n = 2); P15 (n = 3); P17 (n = 3); P18 (n = 2); P20 (n = 1); P22 (n = 2); P28 (n = 1); P31 (n = 2); P32 (n = 1); P36 (n = 1); P38 (n = 2); P40 (n = 1); P42 (n = 2); P44 (n = 3). Of the 57 animals used in this study, 17 were used for both classification and reconstructions, three were used solely for classification, 21 were used solely for reconstructions, and four were used solely for figures. The remaining 12 were not used because of poor Golgi impregnation (see below).

P0 animals were euthanized within 5 hours after birth. All pups were housed with their dam and littermates. Rats were housed with a 12-hour light/dark cycle with ad libitum access to food and water. All methods were approved by the Yale Animal Care and Use Committee and were in accordance with NIH guidelines.

Golgi material

Tissue preparation. Animals from P0 to P17 were anesthetized with halothane (3–5 mL, inhalation). Subjects older than P17 were anesthetized with Nembutal (80–90 mg/kg, i.p.) and perfused transcardiacally with 0.9% saline. Immediately following anesthesia or perfusion, animals were decapitated and the brain was rapidly

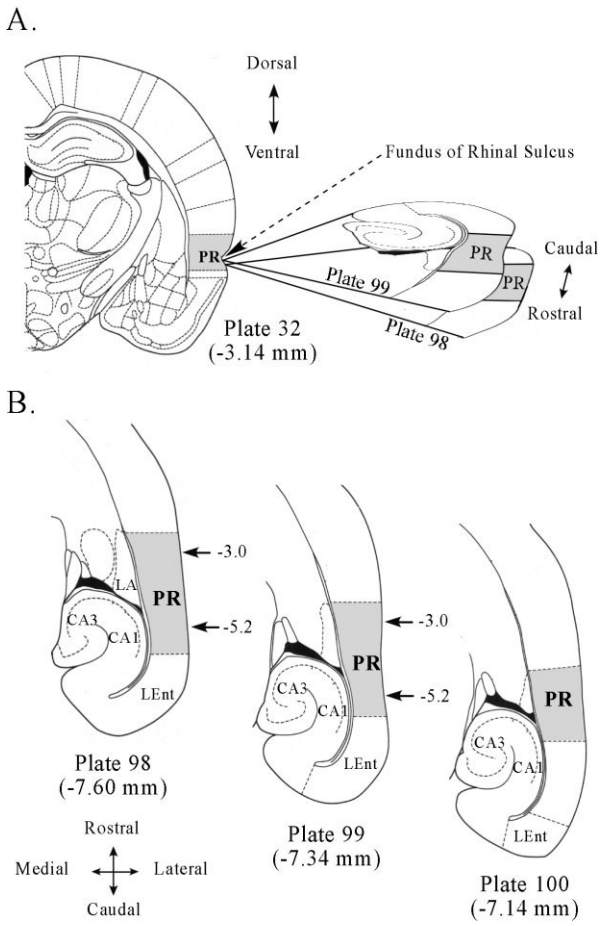

Fig. 1. Anatomical borders of rat perirhinal cortex (PR) in stereotaxic coordinates. **A:** Diagram of a coronal section (left) showing the dorsoventral locations of horizontal sections (right) that correspond to plates 98 and 99 of Paxinos and Watson (1998). Both of these plates represent sections that are near or below the fundus of the rhinal sulcus, which guarantees that they are from PR and not from auditory neocortex. **B:** Horizontal diagrams of PR at three dorsoventral locations. Data from Golgi-impregnated tissue were only collected from sections corresponding to plates 98 and 99. Data collection was limited to the rostrocaudal extent of PR indicated by the arrows (see Furtak et al., 2007). Modified and reprinted from the Rat Atlas by George Paxinos and Charles Watson, Figures 32, 98–100. Copyright (1998), with permission from Elsevier.

removed. Brains were incubated for 6–17 days in a modified Golgi-Cox solution containing (weight-to-volume ratio) 1.042% potassium dichromate, 1.042% mercuric chloride, and 0.833% potassium chromate (Gibb and Kolb, 1998). At least 7 days later, brains were transferred to a 30% sucrose solution in order to increase pliability. Both incubations were shielded from light.

As in our neurophysiological studies of PR brain slices (Moyer and Brown, 1998, 2007), the hindbrain was first removed before sectioning. The transverse dissection plane spared posterior cortex and passed anterior to the cerebellum and the interpeduncular nuclei. Horizontal slices (200 μm thick) were then collected with a vibratome, starting with the ventral surface of the brain (Fig. 1A). Sections were blotted onto gelatin-coated slides using moist filter paper to facilitate adherence to the slides. Sections were reacted in accordance with a previously published protocol (Gibb and Kolb, 1998). Briefly, sections were placed in a series of washes: deionized water (dH_2O) for 1 minute; ammonium hydroxide for 30 minutes in the dark; dH_2O for 1 minute; Kodak Fix for Film for 30 minutes in the dark; dH_2O for 1 minute; 50% ethanol for 1 minute; 70% ethanol for 1 minute; 95% ethanol for 1 minute; 100% ethanol for 5 minutes; fresh 100% ethanol for 5 minutes; and rinsed in a solution of equal parts of chloroform/HemoDe or Citrisolv (Fisher Scientific, Pittsburgh, PA)/ethanol for 15 minutes. Sections were mounted in Permount (Fisher Scientific) and coverslipped. A portion of the slides were placed in a desiccator for 1 month to decrease background staining.

A subset of tissue was counterstained for Nissl for verification of laminar borders. For these reactions, rats were perfused intracardially with 0.1 M phosphate buffered saline (PBS; pH 7.4) and brains rapidly removed and rinsed with 0.1 M PBS (to remove blood). Brains were then blocked to remove the frontal lobe and cerebellum and placed into a solution of potassium chromate, mercuric chloride, and potassium dichromate (<2% w/v; FD NeuroTechnologies, Ellicott City, MD; Rapid GolgiStain KitT, cat. no. PK401). The Golgi impregnation solution was prepared 24–48 hours prior to use. After 24 hours, the brains were transferred to fresh impregnation solution where they remained for an additional 20 days. Brains were then transferred to a cryoprotectant solution (FD Neurotechnologies, Rapid GolgiStain KitT) and stored at 4°C overnight. The next day the cryoprotectant solution was changed and the brain stored at 4°C for 1–5 additional days. Brains were frozen and 120 μm horizontal sections were cut using a cryostat. Sections were mounted onto gelatin-coated slides and allowed to dry overnight at room temperature. Sections were then rinsed in distilled water, placed into the developing solution (FD Neurotechnologies, Rapid GolgiStain KitT) for 10 minutes, and rinsed in distilled water. For counterstaining, sections were incubated in 0.5% thionin (Sigma, St. Louis, MO, cat. no. T7029) for 2–3 minutes, rinsed in cold tap water, dehydrated, cleared in xylene, and coverslipped with Permount. Alternate sections that were not counterstained were dehydrated, cleared, and coverslipped as described above.

An additional brain was stained for Nissl using Cresyl Violet. For this stain, rats were perfused intracardially with 0.1 M PBS followed by 4% paraformaldehyde. The brain was removed, placed in 4% paraformaldehyde for 24 hours, and then transferred for 3 days to a 30% sucrose solution for cryoprotection. Seventy micron horizontal sections were cut using a freezing microtome. Sections were mounted on gelatin-coated slides and allowed to dry overnight at room temperature. The next day sections were placed in the following order of solutions: 100% ethanol for 1 minute; 95% ethanol for 1 minute; 70% ethanol for 1 minute; 50% ethanol for 2 minutes; Cresyl Violet for 4 minutes; 50% ethanol for 30 seconds; 70% ethanol for 30 seconds; 95% ethanol for 1 minute; 100% ethanol for 1 minute; Citrisolve for 5 minutes; and fresh Citrisolve for 5 minutes. Subsequently, slides were coverslipped with Permount.

Evaluation of Golgi stain. The quality of the Golgi impregnation had to fulfill specific criteria to be included in the study. Each section was classified into one of three groups based on the quality of staining. Well-stained cells

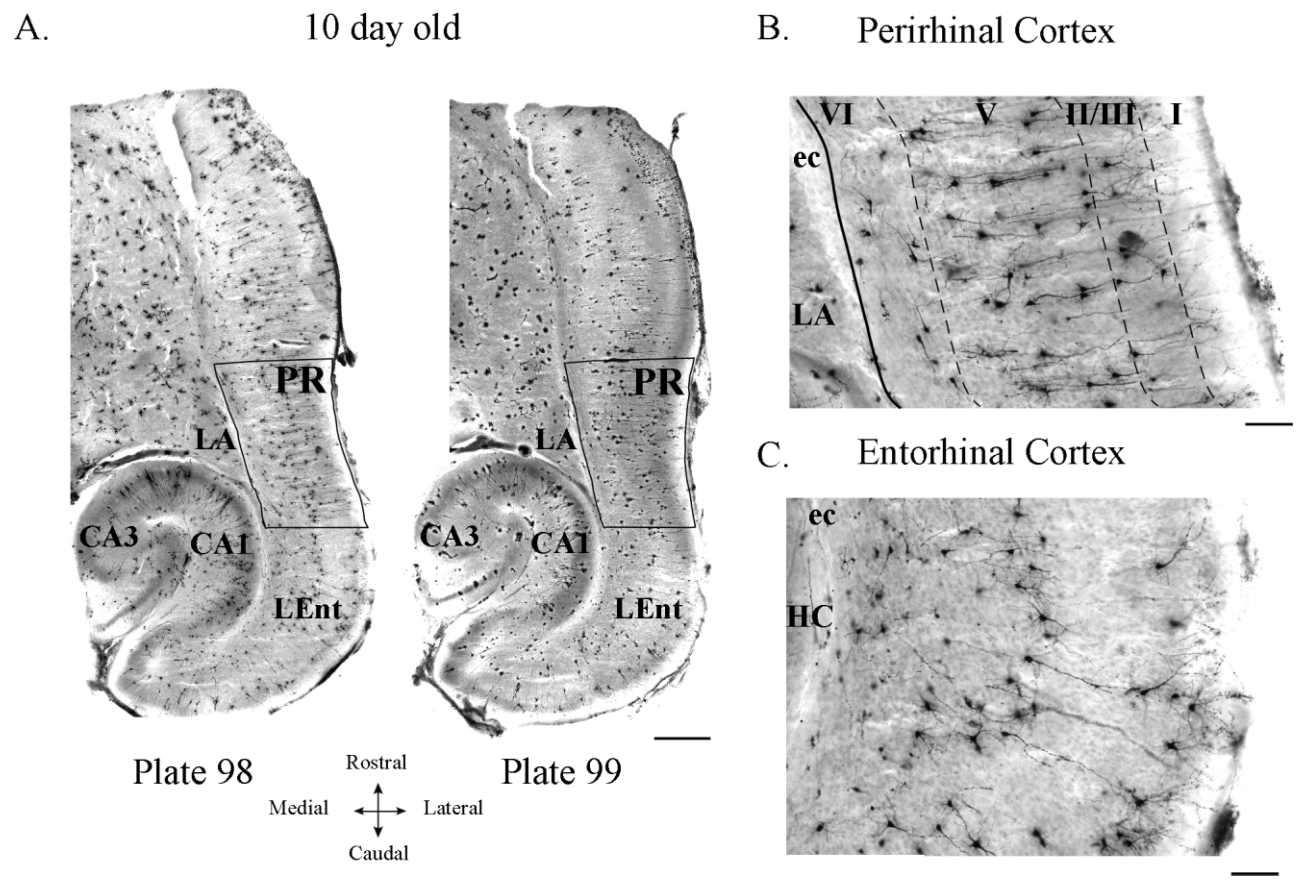

Fig. 2. Golgi-impregnated tissue from a postnatal day 10 (P10) rat. **A:** Two horizontal sections, taken from the same animal, corresponding to plates 98 and 99 of Paxinos and Watson (1998). The outlined area shows the rostrocaudal limits of perirhinal cortex (PR) used in the present study. Objective magnification: 2.5×. **B:** A higher-magnification image of PR, taken from plate 98 in Part A. Dashed lines delineate layers within PR. The solid line indicates the border of PR with the external capsule (ec). Objective magnification: 10×. **C:** A higher-magnification image from the lateral entorhinal cortex (LEnt) from plate 98 in Part A. None of the obvious laminar distribution of cell types, described for PR, was observed in LEnt. Objective magnification: 10×. CA1, field CA1 of the hippocampus; CA3, field CA3 of the hippocampus; HC, hippocampal formation; LA, the lateral nucleus of the amygdala. Scale bars = 500 μm in A; 100 μm in B,C.

were completely impregnated with a dark, ink-like impression throughout the soma and dendrites. Moderately-stained cells were characterized by a dark stain in the soma and the proximal dendrites. The stain at the distal regions of the dendrites was gray, with visible Golgi particles. Poorly-stained cells were marked by a light grayish soma with visible Golgi particles and no dendritic staining. The quality of Golgi impregnation tended to be relatively consistent within each section. Morphological classifications were conducted on well- and moderately-stained tissue. Neuron reconstructions were conducted exclusively on well-stained tissue. Sections with poorly stained cells were excluded. Due to insufficient staining across multiple sections of a brain, the data from four animals were excluded. Subsequent reactions were conducted in the needed age groups until the histological dataset satisfied the acceptance standards.

Coordinates of sampled Golgi-impregnated tissue. The first horizontal section that was retained was ≈1.5 mm ventral to the rhinal sulcus, which is roughly parallel to the plane of these sections. The rhinal sulcus is one of the most distinctive features of the external surface of rat cortex. Sections containing PR were initially identified during sectioning based on the location of the rhinal sulcus. Once all sections were collected and reacted, a more precise delineation of the borders of PR was determined from its unique cellular neuroanatomy as well as by the shape and extent of the hippocampal formation, the anterior commissure, the third ventricle, and the lateral nucleus of the amygdala (LA). The gross neuroanatomical landmarks were compared with plates from a standard rat atlas (Paxinos and Watson, 1998; see Fig. 1).

As sections proceed from the ventral to the dorsal surface of the brain, the hippocampus is the first useful landmark to emerge. In the first section containing the hippocampal formation the dentate gyrus is barely visible. As the ventral hippocampus begins to appear the dentate gyrus assumes a V-like shape. At the most ventral extent of PR the dentate gyrus elongates in a mediolateral direction and assumes a semicircular appearance with a convexity extending out in a caudal direction (Fig. 1B, also Figs. 2A, 3A). At this depth the hippocampal formation as a whole becomes circular and filled out, corresponding to plate 98 of the stereotaxic rat atlas (Paxinos and Watson, 1998; see Fig. 1B). Additionally, LA has an obvious triangular shape (Fig. 1B), which is easily discerned even in

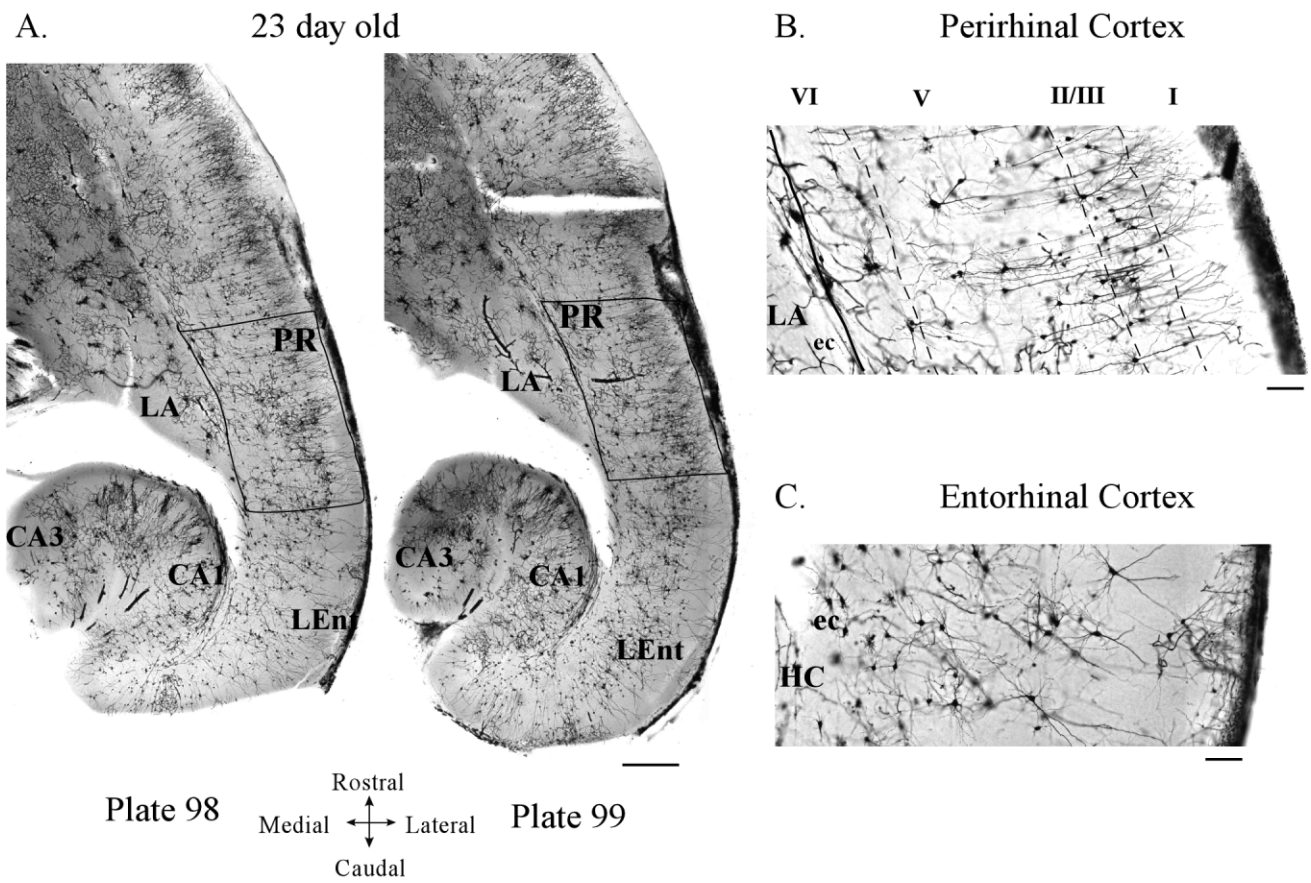

Fig. 3. Golgi-impregnated tissue from a postnatal day 23 (P23) rat. **A:** Two horizontal sections, taken from the same animal, corresponding to plates 98 and 99 (Paxinos and Watson, 1998). The outlined area shows the rostrocaudal limits of perirhinal cortex (PR) used in the present study. Objective magnification: 2.5×. **B:** A higher-magnification image of PR from plate 98 in Part A. The dashed lines delineate cortical layers (see text for detail). The solid line indicates the border of PR with the external capsule (ec). Notice the much more elaborate dendritic branching compared to the images from postnatal day 10 (Fig. 2B). Some features that distinguish PR layers in Golgi-stained sections include the following: layer I is essentially cell free; layer II/III contains the highest density of small pyramids; layer V contains many large pyramidal neurons at a much lower density than in layer II/III; and layer VI neurons have an obviously horizontal organization (also Figs. 2B, 4). Objective magnification: 10×. **C:** A higher-magnification image of lateral entorhinal cortex (LEnt) from plate 98 in Part A. Entorhinal cortex shares none of the laminar organization that was just described for PR. Objective magnification: 10×. See Figure 2 for additional abbreviations. Scale bars = 500 μm in A; 100 μm in B,C.

unstained living brain slices (Moyer and Brown, 1998). The lateral nucleus of the amygdala continues to be obvious in sections corresponding to plate 99, but its size diminishes in sections corresponding to plate 100 (Fig. 1B). As the sections precede dorsally the dentate gyrus narrows into a U-shape and the hippocampal formation becomes an elongated oval. The depth at which the hippocampal formation becomes elongated corresponds to plates 100–101 of the stereotaxic rat atlas (Paxinos and Watson, 1998; see Fig. 1B).

These changes in the appearance of the hippocampal formation coincide with an obvious shortening of the third ventricle. In sections ventral to PR, the third ventricle is evident along about 60% of the midline of the included tissue. As PR begins to emerge (corresponding to plate 98), the third ventricle shortens to about 25% of the length of the tissue at the midline and the anterior commissure becomes visible. The anterior commissure remains visible throughout sections that contain PR. At the most dorsal extent of PR the anterior commissure extends across the midline into both hemispheres. These anatomical features and their relative progression were consistent in all age groups. Further delineation of PR, based on Golgi-impregnated sections, is furnished in the Results section (see Nomenclature in Results).

The morphological classifications were confined to the first section within plate 98 and the first section within plate 99 (Figs. 1–3) of the rat stereotaxic atlas (Paxinos and Watson, 1998). The cell classifications used both hemispheres of these two brain slices in each animal. The 2D and 3D reconstructions were conducted on any section within plates 98 and 99. Depending on the age of the animal, this included two to three sections. All classifications and reconstructions were based on sections at or ventral to the fundus of the rhinal sulcus (Fig. 1A), thereby eliminating any possibility of including auditory cortex. The stereotaxic coordinates (relative to bregma) of the rostrocaudal extent of PR that was included in the data analysis ranged from −3.0, which is slightly caudal to the rostral tip of LA, to −5.2 mm, which corresponds to

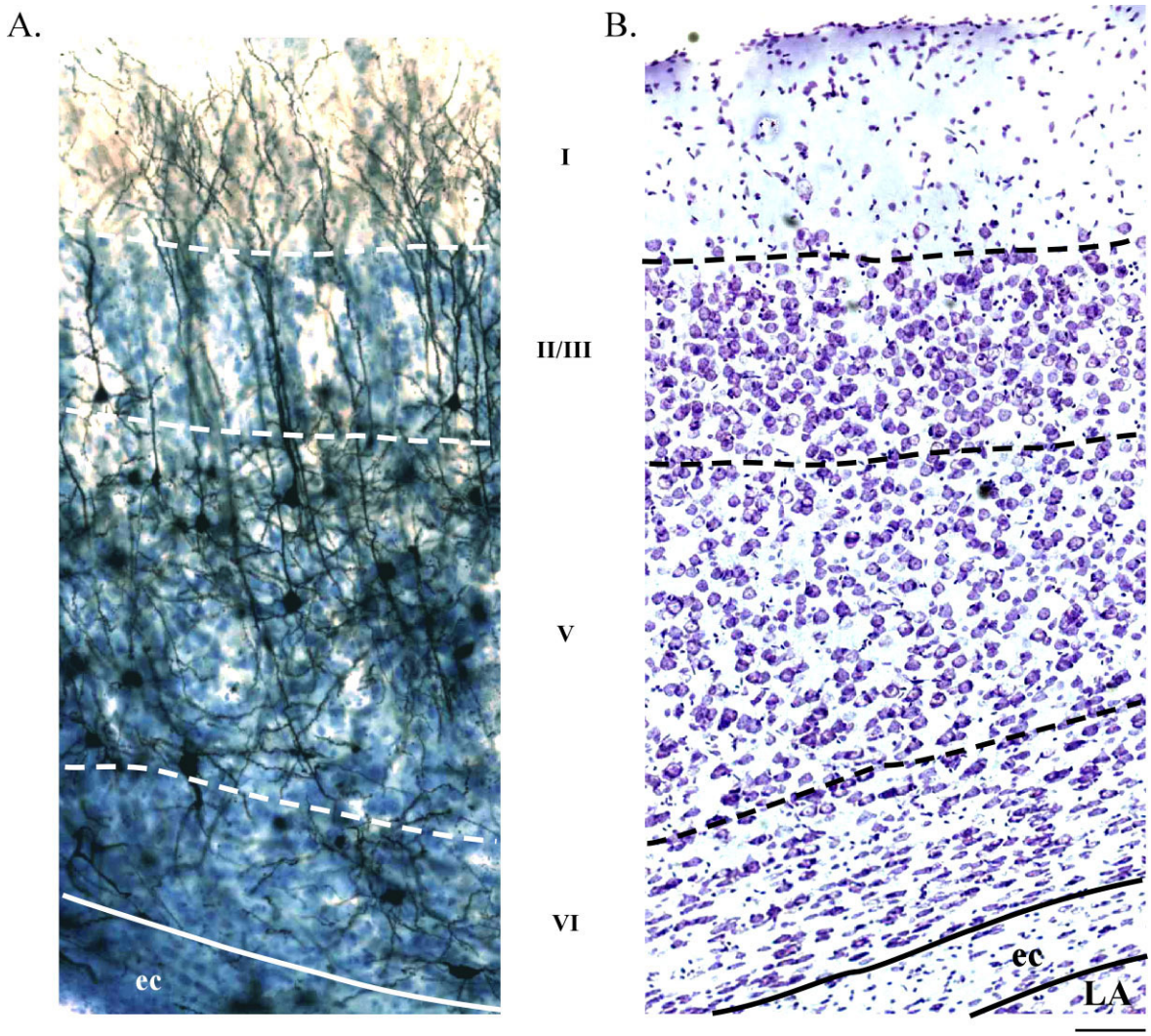

Fig. 4. Laminar organization of perirhinal cortex (PR). The same laminar organization is evident in Golgi- and Nissl-stained tissue. The illustrated sections are taken from horizontal sections corresponding to plate 98 (Paxinos and Watson, 1998). The dashed lines delineate cortical layers (see text for details). The solid lines indicate the border between PR and the external capsule (ec). In part B a solid line also separates ec from the lateral border of the lateral nucleus of the amygdala (LA). **A:** Golgi-impregnated tissue that was counterstained for Nissl from a postnatal day 36 (P36) rat. No neurons were labeled in PR layer I. Layer II/III contained the highest density of small pyramids. **B:** Nissl-stained tissue from an adult animal showing the same laminar boundaries. Features that easily distinguish layers include the obvious horizontal orientation of layer VI, the highest apparent cell density in layer II/III, the largest cells in layer V, and the infrequent number of cells in layer I. Scale bar = 100 μm.

the more rostral portion of the CA1 region of hippocampus or the rostral tip of the dentate gyrus (Fig. 1B). This region is unequivocally PR, as defined by Burwell and associates (Burwell et al., 1995; Burwell and Amaral, 1998a,b; Burwell, 2001; also see Nomenclature in Results). Every stained cell within the indicated boundaries was examined. Morphological classification and reconstructions used a 40× (NA = 0.85) air objective and air condenser (NA = 0.9).

Laminar distinctions within PR. A total of 6,891 neurons within PR were classified and counted as a function of PR layer (I, II/III, V, VI). The ventral region of PR is agranular and does not contain a layer IV (Burwell et al., 1995; Burwell and Amaral 1998a,b; Burwell, 2001). Layers I, II/III, V, and VI were discriminated using multiple criteria (Figs. 2–4). Layer VI was clearly distinguishable from layer V based on the cell orientations (Figs. 2B, 3B, 4). Overall, cells within layer VI were oriented parallel to the pial surface and the external capsule. In layer V, most pyramidal cells were oriented perpendicular to the pial surface and the external capsule (ec; see Figs. 2B, 3B, 4). In addition, the structure of pyramidal neurons distinguished layer V from layer II/III.

Layer II/III pyramidal cells had a short apical dendrite with numerous arborizations along its shaft, had extensive basilar dendrites, and had abundant spines. In contrast, layer V pyramidal cells had a long apical dendrite with a few fine secondary processes along its shaft, had a prominent apical tuft, and had less extensive basilar dendrites (Figs. 2B, 3B; cf. Faulkner and Brown, 1999; Moyer

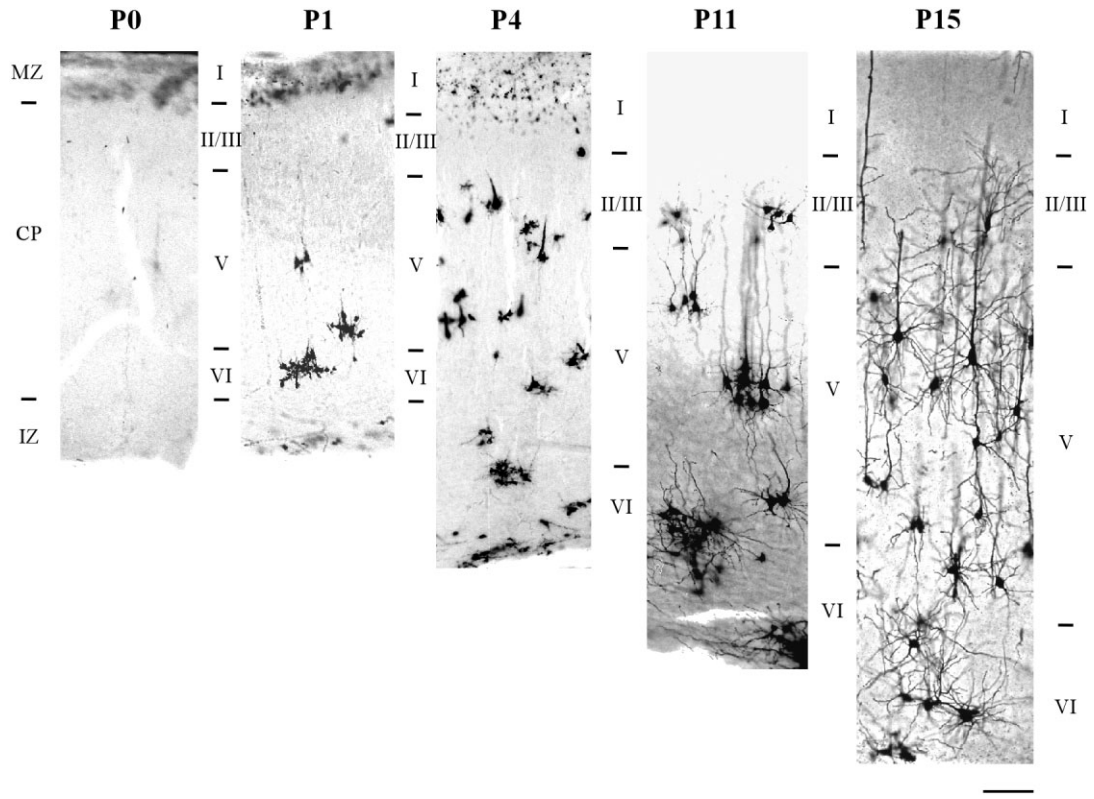

Fig. 5. Laminar development as revealed in Golgi-impregnated tissue in perirhinal cortex. At postnatal day 0 (P0) and P1 tissue is divided into the marginal zone (MZ), the cortical plate (CP), and the intermediate zone (IZ). At these ages layers cannot yet be distinguished. However, note that layers were superimposed at these age groups to preserve positional information (also see Materials and Methods). To the right of each photograph, perirhinal layers are shown for each age group. There were no cells present at P0. The inside-out pattern of development is evident by P1. Aggregates of Golgi-impregnated neurons are present in tissue from P1 to P11. Scale bar = 100 μm.

et al., 2002). No attempt was made to separate layer II from layer III. There was no obvious or natural distinction between layers II and III in Golgi-impregnated material. The same conclusion was previously reached based on neurons that were reconstructed following WCRs and also based on real-time imaging of the tissue in living brain slices using infrared illumination and differential-interference-contrast optics (Moyer and Brown, 1998, 2007; Faulkner and Brown, 1999; Beggs et al., 2000). Layer II/III was distinguished from layer I by the presence of upright pyramidal cells. These criteria lead to the same division of cortical layers based on a subset of Nissl-stained sections (Fig. 4). The laminar distinctions in the present study are consistent with those of Burwell (2001).

As in other studies of neocortical development (Miller, 1981), identification of distinct laminae was not possible until P4. To characterize the position of cells at P0 and P1, the cortical plate (CP) was artificially subdivided into three regions, with relative sizes corresponding to what would become layers II/III, V, and VI (Fig. 5). The most lateral area was assigned to the marginal zone (MZ), which later develops into layer I (Fig. 5; Boulder Committee, 1970). Graphs that include positional information about cells at P0 and P1 assigned them to a virtual layer in this manner for the purpose of elucidating changes in position and spatial continuity with later stages of development (Fig. 5).

Cellular reconstructions and photomicrographs of Golgi-impregnated tissue. 3D reconstructions were performed on 398 neurons that were representative of each cell class (see Morphological Classification Scheme). Somatic area and dendritic length measurements were obtained using Neurolucida (MicroBrightField, Colchester, VT). After restricting the rostrocaudal extent of the analysis (−3.0 to −5.2 mm relative to bregma, see Fig. 1B), 245 reconstructions were included in the 3D dataset presented here. As previously mentioned, reconstructions were performed with a 40× air objective (NA = 0.85) and an air condenser (NA = 0.9). Reconstructed cells had to be fully discernible and to have no more than two unnatural dendritic terminations. Unnatural dendritic terminations were not accepted on primary dendrites. These selection criteria for reconstructions might be expected to underrepresent the length of any dendritic arbors that were extensive along the dorsoventral axis relative to the thickness of the sections (200 μm). Any such bias should be greatest for the large multipolar neurons, whose dendritic arbor was not specifically organized in any plane. By contrast, the dendrites of pyramidal neurons tended to be contained in either the mediolateral or rostrocaudal plane of the horizontal section. The smaller cell classes should have been least affected because the spread of their dendrites in any plane was very small relative to the thickness of the sections. Possible effects of the selection crite-

ria on specific inferences from the reconstructions are further considered later (see Discussion).

For illustrations of Golgi-impregnated material, photomicrographs were obtained using a Zeiss Axioskop (Carl Zeiss, Thornwood, NY) equipped with either a Zeiss Axiophot module for film-based photography or a Neurolucida system with an Optronics Microfire digital microscope CCD camera (MicroBrightField) for digital-based photography. Black-and-white film-based photomicrographs were scanned at 1536 × 1024 dpi and saved as jpeg files by Imag'In Café & Studio (New Haven, CT). For digital-based photomicrographs, black-and-white frames were captured at 1600 × 1200 dpi and saved as jpeg files with Neurolucida. Images were adjusted for brightness and contrast using Canvas 8.0 (Deneba Software, Miami, FL). Composites of multiple photomicrographs and the addition of text were made using Canvas 8.0.

Morphological classification scheme

Cells were classified into one of 15 groups based on somatic form, dendritic arbor, and orientation. Classifications based on axonal arborization (Martinotti, basket, double-bouquet, and chandelier cells) were not included due to poor axonal staining, which is typical of Golgi-Cox impregnation. The classification included five types of pyramidal neurons (upright, bifurcating, inverted, horizontal, and oblique) and 10 types of nonpyramidal neurons (bipolar, bitufted, Cajal-Retzius, cone, fusiform, multipolar, neurogliaform, stellate, small round, and tripolar).

Pyramidal neurons. Pyramidal cells are characterized by a triangular-shaped soma and a single, dominant, apical dendrite. The apical dendrite arises from the apex of the soma and gradually tapers as it extends away from the soma. Copious, thinner, basilar dendrites develop from the base of the soma (Fig. 6). The diameter of the apical dendrite is thicker than any other dendrite. Typically, a small portion of the axon can be visualized as it emerges from the base of the soma (Fig. 6).

The most common of the five types of pyramidal neurons is the *upright* pyramidal cell. Upright pyramidal cells have an apical dendrite that extends perpendicularly toward the pial surface. After extending into layer I or layer II/III, the apical dendrite branches many times to form the apical tuft. *Inverted, horizontal,* and *oblique* pyramidal cells are structurally similar to upright pyramidal cells. In these cell types, the apical dendrite extends, respectively, either in a medial direction (perpendicularly away from the pial surface), in a horizontal (rostrocaudal orientation) direction parallel to the pial surface, or at an oblique angle to the pial surface (Fig. 6). These variants of pyramidal cells tend to have less distinctive apical tufts, but they have other pyramidal characteristics, such as a dominant apical dendrite that extends farther than other dendrites, and an axon that arise from the somatic base, and spines (Fig. 6). *Bifurcating* pyramidal cells have a single apical dendrite arising from the apex of the soma that branch, after a short distance from the soma, into two, equally thick, gradually tapering apical dendrites (Fig. 6). Each branch of the apical dendrite has a distinct tuft.

Nonpyramidal neurons. The 10 types of nonpyramidal neurons, described here in alphabetical order, constitute a structurally heterogeneous cell category (Fig. 7). *Bipolar* cells have an elongated, spindle-shaped soma. A single dendrite arises at each end of the soma. Dendrites split once or twice and extend in a long, narrow dendritic tree (Fig. 7; Feldman and Peter, 1978; Peters and Regidor, 1981; Peters, 1984), which can be aspiny or sparsely spiny. This classification was always restricted to cells with two primary dendrites. *Bitufted* cells have sparsely spiny dendrites extending from opposite poles of a spindle-shaped soma. Unlike bipolar cells, bitufted cells can have more than one dendritic head (a thick dendritic process arising from the soma; see Millhouse and DeOlmos, 1983) at each pole. After extending only a short distance, the dendrite branches many times into tufts (Fig. 7; Feldman and Peters, 1978; Peters and Regidor, 1981).

Cajal-Retzius cells have numerous short and long branchlets. These finely-beaded branchlets extend toward the lateral surface. There is also a thick process that extends medially. Several horizontal dendritic collaterals arise from this descending process. In the bottom half of layer I the descending process converts into a long horizontal axon. The dendrites of these cells turn into axons (Ramón y Cajal, 1911) that stain with Golgi-Cox (in contrast to axons of other cells). These cells are found at the pial surface and are unique to the marginal zone or "layer I" in young animals (Marin-Padilla, 1984). Cajal-Retzius cells are less common in association cortices and are usually observed in primary sensory areas such as visual cortex (Marin-Padilla, 1984).

Cone cells have a spindle-shaped soma. On one end of the soma are two to three dendritic heads. Each dendritic head divides a short distance from the soma into several, thinner, dendritic processes. These thinner processes extend out in a cone-like shape. There is little spatial overlap between the branches of each dendrite. On the opposite end of the soma there is typically one, narrow, dendritic process that has few if any secondary processes. Dendrites were usually aspiny. Within PR these cells have only been reported in layer VI (Faulkner and Brown, 1999; McGann et al., 2001). They have also been reported in the amygdala (Millhouse and DeOlmos, 1983).

Fusiform cells have a spindle-shaped soma. Unlike bipolar cells, fusiform cells always have at least three sparsely spiny dendrites that arise from or close to the two somatic poles. The primary dendrites only branch a few times. Fusiform cells have dendritic arbors that are longer and narrower than a bitufted cell (Fig. 7). *Multipolar* cells have spiny dendrites that arise from any part of the soma, such that there is no preferred site of origin. The dendrites radiate in all directions with no sense of orientation (Fig. 7). *Neurogliaform* cells have a spherical soma. Numerous short, finely beaded dendrites arise from all sides of the soma (Fig. 7). The dendrites have a strictly local arborization (Jones, 1984).

Small round cells have one or two short, aspiny dendrites that originate from a small soma (5–10 μm). These aspiny dendrites extend a very short distance from the soma (Fig. 7). Small round cells can be visually identified in living brain slices and always exhibit fast-spiking properties (Faulkner and Brown, 1999; McGann et al., 2001). *Stellate* cells have a spherical soma of medium-size (12–22 μm diameter). Four to six aspiny dendrites produce a star-like arbor (Fig. 7). Some classification schemes treat stellate cells as an aspiny subclass of small multipolar cells or distinguish between spiny and aspiny stellate cells. In the present study, we consider stellate cells to be distinct from multipolar cells, which are large and spiny.

Tripolar cells have triangular-shaped somas with one dendritic process extending from each of the three conver-

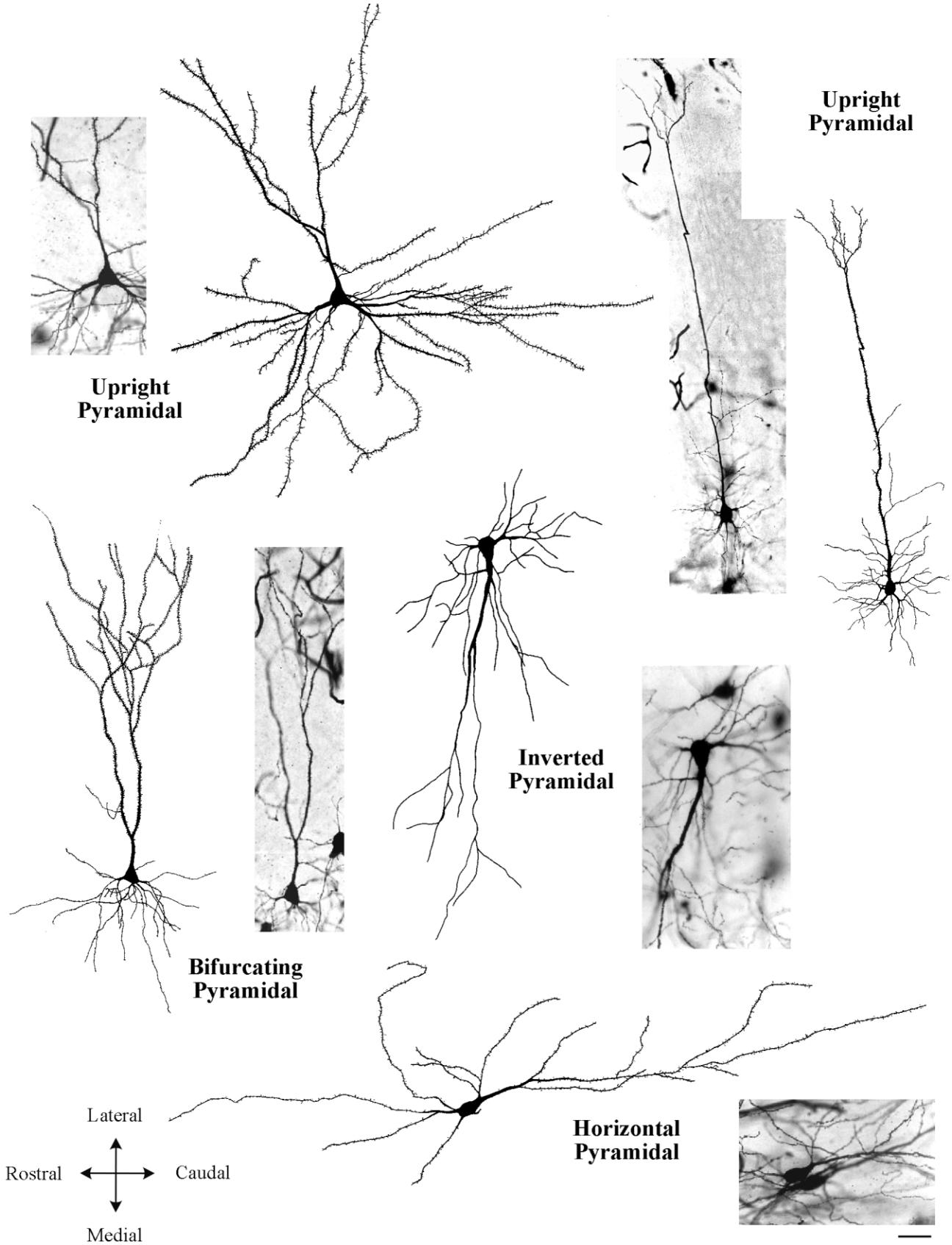

Fig. 6. Four types of Golgi-impregnated pyramidal neurons in rat perirhinal cortex. Photographs are accompanied by camera lucida reconstructions. Scale bar = 50 μm.

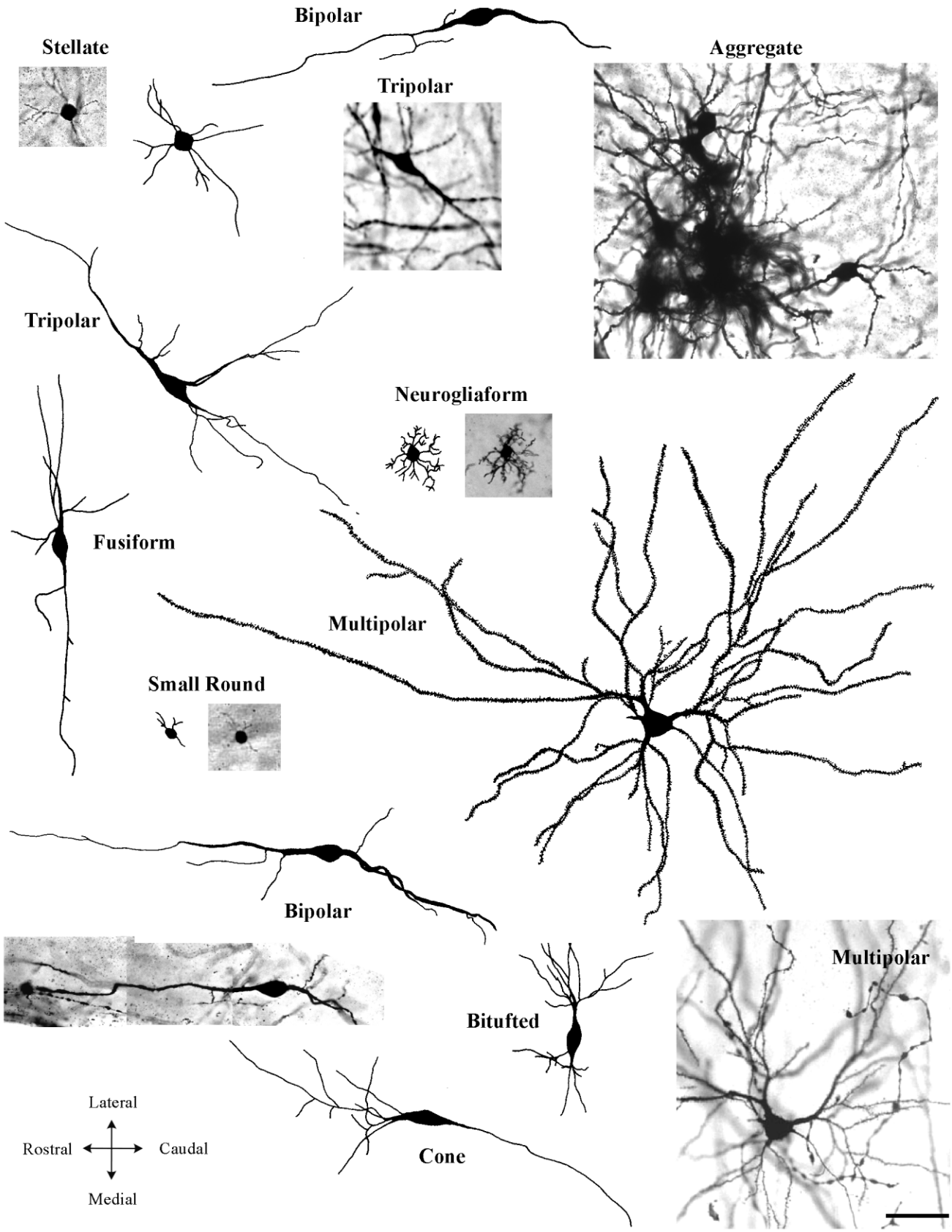

Fig. 7. Nine types of Golgi-impregnated nonpyramidal neurons and an example of an aggregate of stained cells in rat perirhinal cortex. Scale bar = 50 μm.

gence points. Two of the dendritic processes extend from opposite ends of the soma. These two processes give a sense of an orientation to the cell (Fig. 7). Dendrites of tripolar cells were usually sparsely spiny. The term *aggregate* is used to describe clusters of three to seven Golgi-impregnated neurons. Because of their close proximity to each other, individual neurons within an aggregate cannot be readily distinguished or classified reliably. Aggregates of Golgi-impregnated neurons have been reported during the early development of visual cortex (Miller, 1981). The number of aggregates was recorded as a function of layer and age.

RESULTS

Nomenclature

Data were collected from an area of PR that was markedly ventral to its border with the temporal association cortices and also well within the rostrocaudal extent of what is widely considered PR (Burwell et al., 1995; Burwell and Amaral, 1998a,b; Burwell, 2001). Recall that all data were from sections at or ventral to the fundus (Fig. 1A), thereby excluding auditory cortex. For this reason, here we emphasize the distinction between ventral PR and its border with the lateral EC. Several features distinguished PR from EC. Layer I, which rarely contained Golgi-impregnated cells, was larger in PR than in EC (Figs. 2, 3). This fact has been noted previously (Burwell et al., 1995; Burwell and Amaral, 1998a,b). Approximately 50% of Golgi-stained cells in PR layer II/III consisted of small upright and frequently bifurcating pyramidal cells (Figs. 2B, 3B). By contrast, in layers II and III of EC the vast majority of stained cells were multipolar neurons (Figs. 3, 4). Note, however, that this distinction is more easily visualized in EC of mature tissue (P23) than in young tissue (P10; Figs. 2C, 3C). These multipolar cells presumably contribute to the clusters of cells that are referred to as "islands" and are typically used to categorize EC (Ramón y Cajal, 1911). Islands were not visible in Golgi-stained sections of PR.

In layer V of PR, pyramidal cell bodies are larger than in layer II/III. The apical dendrites of layer V pyramidal neurons extend a greater distance toward the pial surface compared to pyramids in layer II/III (Figs. 2B, 3B). These large layer V pyramidal cells are not observed in EC in Golgi-stained material (Figs. 2C, 3C). Previous studies have reported similar findings in Nissl-stained material (Burwell et al., 1995; Burwell and Amaral, 1998a,b; Burwell, 2001). Collectively, the pyramidal cells in layers II/III and V of PR have an obvious "radial" orientation in which the dendrites tend to be directed toward the pial surface. This radial orientation ends abruptly at layer VI of PR, where the cells have an obvious horizontal orientation (parallel to the pial surface; see Figs. 2B, 3B). The laminar distribution and orientation of various cell types in Golgi-impregnated sections, in conjunction with gross neuroanatomical landmarks, enable unequivocal distinctions between PR and surrounding cortices (see Materials and Methods for further description).

Development of perirhinal cortex

Perirhinal cortex develops in the "inside-out" pattern that has been described in neocortical areas. Golgi-impregnated neurons first proliferated in deep layers and were rarely present in superficial laminae until P4 (Fig. 8; also Fig. 5). There were a total of three Golgi-impregnated neurons at P0. Two of these cells were Cajal-Retzius cells and were located in the marginal zone of the same section. At P1 the majority of cells were deep within the cortical mantle, corresponding to layer VI (Fig. 8; also Fig. 5). By P4 nearly all of the stained neurons were in layers V and VI (Figs. 5, 8). From P6 through P45, layer V contained 65–75% of the Golgi-impregnated neurons. This large percentage partially reflects the fact that layer V is roughly twice as large as any other layer (Fig. 5). Layers II/III and VI each contained between 10–15% of stained neurons. Golgi-impregnated cells were rarely located in layer I (≈1%).

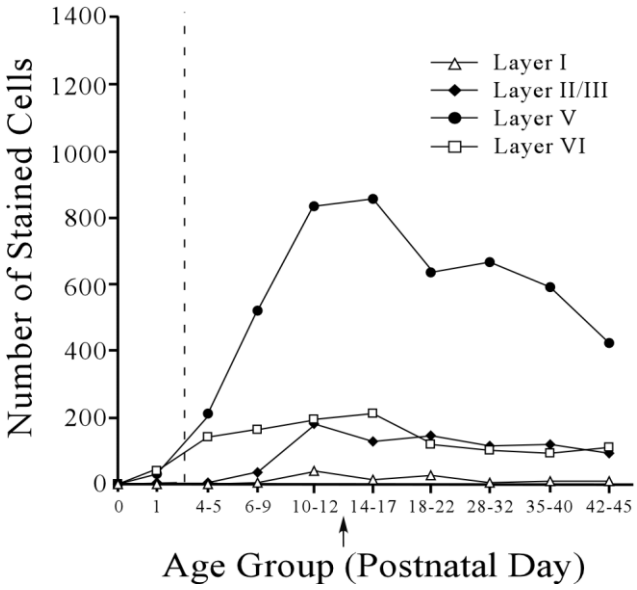

Fig. 8. Total number of Golgi-stained neurons in rat perirhinal cortex (PR) as a function of age and PR layer. For each layer of perirhinal cortex the total number of stained cells (y-axis) is plotted as a function of age group (x-axis, n = 2 per age group). Notice that Golgi-impregnated cells are observed in deep layers (V and VI) before superficial layers (I and II/III), reflecting an inside-out pattern of development. Stained cells are not present in layers I and II/III until P10. This is similar to development in neocortical areas. Cortical lamination is not discernable to the left of the vertical broken line (see text). Arrow denotes time of eye-opening.

The largest neurons proliferated before smaller ones. The vast majority of cells observed prior to P6 were the two largest morphological types—multipolar and pyramidal cells (Fig. 9A, Table 1). Pyramidal neurons were the most abundant cell type throughout development, comprising roughly half the Golgi-impregnated cells in PR. There was no apparent size-based sequencing among the subset of small nonpyramidal cells (Fig. 9B, Table 1). The small round neurons, the most diminutive of nonpyramidal cells, proliferated roughly in parallel with tripolar neurons (Fig. 9B, Table 1). Aspiny stellate neurons were the last cells to develop. Note that the development of aspiny stellate neurons was very different from the small round cells, both of which are presumed to be inhibitory (Fig. 9B).

Throughout development the majority of the pyramidal neurons were upright pyramidal cells (Fig. 10, Table 1).

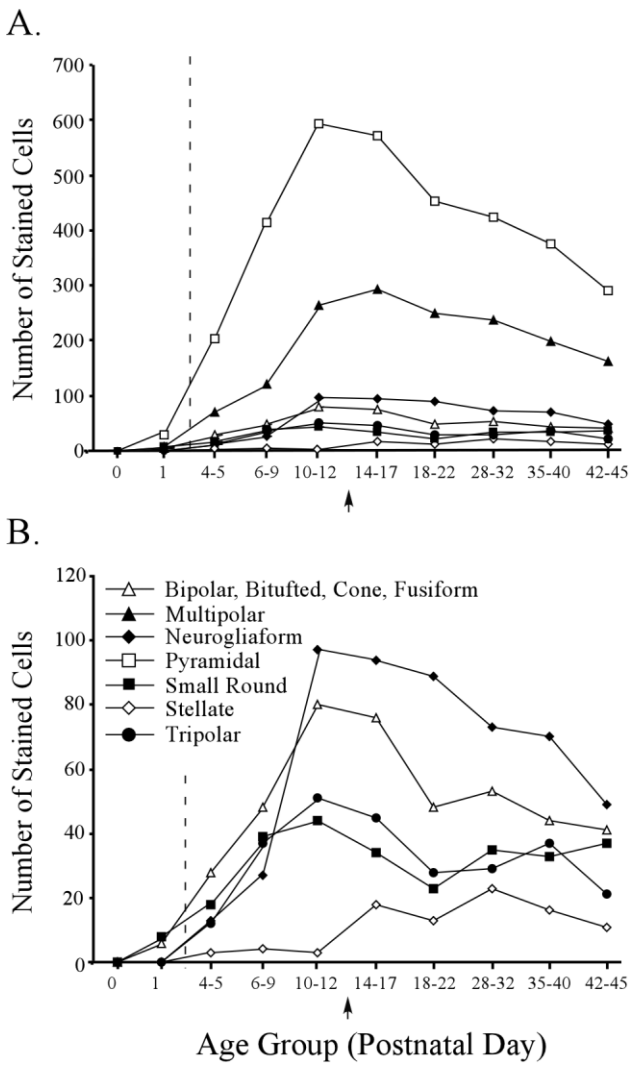

Fig. 9. Changes in the number of Golgi-stained neurons in rat perirhinal cortex (PR) as a function of cell class. The total number of stained cells (y-axis) for each cell class is plotted as a function of age group (x-axis, n = 2 per age group). For graphical simplicity, all five classes of pyramidal types are combined and four of the nine classes of nonpyramidal neurons (bipolar, bitufted, cone, and fusiform) are pooled. Arrows denote time of eye-opening. **A:** Changes in the numbers of each cell class as a function of age in PR. Pyramidal and multipolar cells, the two largest cell classes, are the first cell types to emerge during development in PR. **B:** An expanded view of the five less common classes of perirhinal neurons (from A) as a function of age. Note that aspiny stellate cells, which are presumably inhibitory and one of the smallest cell classes, are the last to develop in PR.

Among the remaining types of pyramidal cells, horizontal pyramidal cells were observed the earliest. Recall that the horizontal pyramidal cells were largely in layer VI, which develops earliest (Figs. 5, 8). Horizontal, inverted, bifurcating, and oblique pyramidal cells together accounted for 8% of the total number of Golgi-impregnated cells in PR from P18–45. Typically, the apical dendrites of bifurcating pyramidal cells project toward the pial surface (≈96% of bifurcating pyramidal cells), but three bifurcating pyramidal cells were obliquely oriented. These three cells were classified as bifurcating pyramidal cells (rather than oblique pyramidal cells).

3D reconstructions of pyramidal and nonpyramidal cells showed a continuous increase in total dendritic length until P14–17 and P18–22, respectively (Fig. 11A). After P18–22, there was no further increase in the dendritic length in nonpyramidal neurons. In comparison, the total dendritic length continued to increase between P28–32 and P35–40 in pyramidal neurons (Fig. 11A). The standard errors were too large to determine whether there was a sudden "spurt" in the dendritic length of pyramidal cells between P28–32 and P35–40 or a more gradual increase between P18–22 and P35–40 (Fig. 11A). Regression analysis of all cell types from P4–5 to P42–45 suggested a small increase in soma area with increasing age ($r^2 = .07$, $P < 0.01$; Fig. 11B).

Morphological composition of perirhinal cortex

As noted earlier, there were layer-specific differences in the proportion of pyramidal and nonpyramidal neurons. The laminar distributions of pyramidal and nonpyramidal cells and their relative frequencies remained stable after the second postnatal week. Data were therefore combined from P18–45 for further analysis. Layer I was cell sparse. When cells were observed in this layer, they were rarely pyramidal cells (Fig. 12, Table 2). A total of five inverted pyramids were observed in layer I. These five pyramidal cells accounted for only 2% of cells present in layer I (Fig. 12, Table 2). Layers II/III through VI contain a diverse population of pyramidal and nonpyramidal cells. The most prominent laminar difference was the much smaller relative frequency of pyramidal cells in layer VI relative to layers II/III and V (Fig. 12, Table 2). In Layer VI, only 19% of Golgi-impregnated cells were pyramidal neurons (Fig. 12, Table 2). Sixty-seven percent of pyramidal cells located in layer VI were horizontally orientated (parallel to the pial surface). This is a dramatic difference from layers II/III and V, where only 1% of Golgi-impregnated neurons were horizontally orientated pyramidal cells. Overall, PR contained 51% nonpyramidal cells and 49% pyramidal cells.

As previously mentioned, in describing the relative frequency distributions of cell types data were combined from P18–45 because the frequencies remained stable after the second postnatal week. When data were collapsed across PR layers, pyramidal cells were the most frequently observed cell type (49%; Fig. 13). Of these pyramidal cells, 84% were upright pyramidal neurons (radially oriented with the apical dendrite extending toward the pial surface). Multipolar cells accounted for the largest percentage of the nonpyramidal neurons (27% of neurons in PR; Fig. 13). The remaining population of Golgi-stained cells consisted of eight nonpyramidal cell classes. Approximately 9% of Golgi-stained neurons were neurogliaform cells. Small round cells and tripolar cells each accounted for 4% of stained neurons. Bitufted cells and stellate cells, respectively, comprised ≈3% and ≈2% of stained cells. Bipolar cells, cone cells, and fusiform cells each constituted ≈1% of Golgi-impregnated neurons (Fig. 13).

DISCUSSION

This is the first developmental study of the laminar distribution of PR cells types. The results show that PR

TABLE 1. Total Number of Golgi-Impregnated Neurons in Individual Cell Classifications within PR

	Age (Postnatal Day) and Sample Size (n)									
Cell Classification	0 d (n = 2)	1d (n = 2)	4-5 d (n = 2)	6-9 d (n = 2)	10-12 d (n = 2)	14-17 d (n = 2)	18-22 d (n = 2)	28-32 d (n = 2)	35-40 d (n = 2)	42-45 d (n = 2)
Aggregate	—	27	15	41	117	78	26	17	34	21
Bipolar	—	6	13	12	12	12	11	16	5	6
Bitufted	—	—	11	21	45	36	31	26	28	21
Cajal-Retzius	2	—	—	—	—	—	—	—	—	—
Cone	—	—	2	1	10	11	4	5	6	9
Fusiform	—	—	2	14	13	17	2	6	5	5
Multipolar	—	8	70	120	263	292	250	237	199	163
Neuroglia	—	—	13	27	97	94	89	73	70	49
Pyramidal *Total*	1	29	204	413	593	572	452	423	375	291
Horizontal	—	6	26	31	34	33	25	12	17	22
Upright	—	21	153	331	510	487	382	365	307	240
Inverted	—	1	15	22	15	12	20	8	8	8
Bifurcating	1	—	4	23	21	34	19	30	32	18
Oblique	—	1	6	6	13	7	6	8	11	3
Small Round	—	8	18	39	44	34	23	35	33	37
Stellate	—	—	3	4	3	18	13	23	16	11
Tripolar	—	—	12	37	51	45	28	29	37	21
TOTAL	3	78	363	729	1248	1209	929	890	808	634

Dashes represent no cells present in particular cell class at age group.

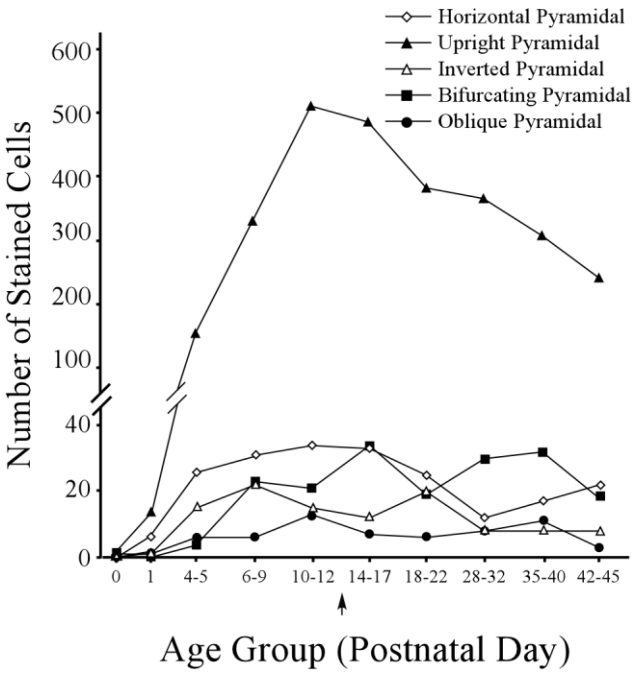

Fig. 10. Distribution of subtypes of pyramidal neurons in rat perirhinal cortex during development. For each different subtype of pyramidal neuron the total number of Golgi-stained neurons (y-axis) is plotted as a function of age (x-axis, n = 2 per group). Upright pyramidal cells are most common. The arrow denotes the time of eye-opening.

develops in a manner similar to neocortical regions that have been comparably studied. However, the morphological and laminar distributions of cell types were unique to PR. The immediate impression of great morphological diversity in PR, relative to neocortex, reflects the greater relative frequency of certain nonpyramidal cell types.

Adherence to developmental laws

Four aspects of PR development, further elaborated below, followed patterns or "laws" that have been established for neocortical development (Uylings et al., 1990; Jacobson, 1991; Price and Willshaw, 2000). First, the total number of cells monotonically increased until P10–12, the time of eye-opening. Second, development proceeded in an "inside-out" fashion, with cells appearing in deep layers before superficial layers. Third, pyramidal and multipolar cells types, the two largest cell types, tended to appear before smaller cells types. Fourth, postnatal dendritic growth patterns were different in pyramidal and nonpyramidal neurons.

Postnatal increase in number of Golgi-stained neurons. A monotonic increase in the number of Golgi-stained cells was observed until P10–12 (Fig. 8). This finding may reflect an increase in the number of neurons during the first postnatal week. Previous studies of other cortical regions report that migration of cortical neurons is not complete until P5 (Berry et al., 1964; Berry and Rogers, 1965; Hicks and D'Amato, 1968; Uylings et al., 1990). There was also an apparent net decrease in the number of Golgi-stained cells after P17. On the other hand, the relative frequency of cell types remained consistent after P17. As with all Golgi methods, we cannot rule out the possibility that some changes in total cell numbers might reflect changes in the efficiency of the stain at different developmental stages. This possibility could be productively explored through stereological analysis of cells labeled with neuron-specific antibodies.

Inside-out laminar gradient. An inside-out pattern was reflected in a mediolateral gradient in which deep layers formed before superficial ones. This pattern was clearly depicted in data from P0 to P10 (Figs. 5, 8). This inside-out gradient is typical in other regions of rat cortex that have been studied (Berry et al., 1964; Berry and Rogers, 1965; Bayer and Altman, 1987; Jacobson, 1991; Price and Willshaw, 2000; Uylings et al., 1990; Uylings, 2000). In general, cortical neurons have been reported to be generated prenatally from embryonic day 16 (E16) until the end of the gestational cycle (E21; Berry et al., 1964). Then, during the first postnatal week, they migrate to their final positions in a layer-specific manner (Berry et al., 1964; Berry and Rogers, 1965; Hicks and D'Amato, 1968; Uylings et al., 1990). One study of neocortex found that postnatal migration was complete by P1–2 for layer

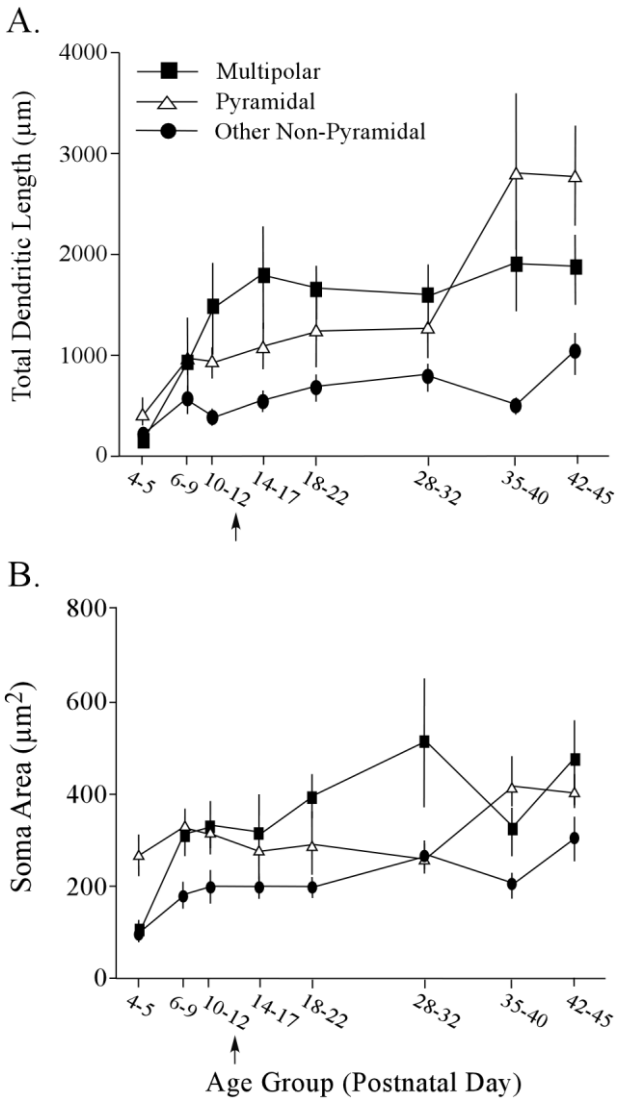

Fig. 11. Morphometric changes in three categories of perirhinal neurons during development. Data from four types of small nonpyramidal neurons (bitufted, cone, neurogliaform, and tripolar) are pooled. **A:** Developmental increases in total dendritic length. **B:** Developmental increases in soma area. Arrows denote approximate time of eye-opening. Error bars are equal to ± 1 SD.

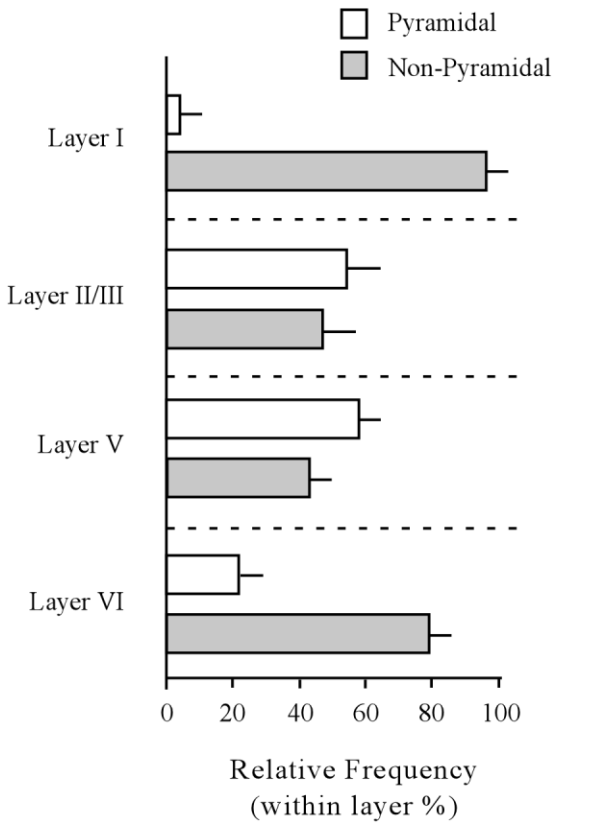

Fig. 12. Relative frequency and laminar distribution of pyramidal and nonpyramidal neurons in rat perirhinal cortex. Data are pooled from eight rats ages P18 through P45 since the laminar distributions do not change after P18. Neurons in layer I and VI have mostly nonpyramidal cell morphologies while those in layer II/III and V have approximately equal proportions of pyramidal and nonpyramidal cell morphologies. Error bars are equal to ± 1 SD.

TABLE 2. Average Percent of Each Cell Classes in Individual Layers from P18-45 Animals

	Perirhinal Layer and Sample Size (n)			
Cell Classification	Layer I (n=8)	Layer II/III (n=8)	Layer V (n=8)	Layer VI (n=8)
Aggregate	3%	1%	2%	13%
Bipolar	8%	1%	1%	2%
Bitufted	1%	3%	3%	4%
Cone	—	—	—	6%
Fusiform	4%	—	—	3%
Multipolar	37%	26%	24%	37%
Neuroglia	23%	11%	8%	6%
Pyramidal (Total)	2%	47%	53%	19%
Small Round	23%	4%	4%	4%
Stellate	—	3%	2%	—
Tripolar	—	3%	3%	6%
TOTAL	100%	100%	100%	100%

Dashes represent no cells present in particular layer.

VI, P2–3 for layer V, and P5 for layer II/III (Berry et al., 1964), which is similar to the development of PR (Fig. 8).

An apparent exception to this inside-out pattern occurred in the present study. Two Cajal-Retzius cells were found on P0 in a superficial region of PR. Both of these Cajal-Retzius neurons were in the same P0 animal in a single section corresponding to plate 99. Cajal-Retzius neurons have been observed in the marginal zone during development (Ramón y Cajal, 1911). The marginal zone is present prior to the formation of the cortex in the developing rat. Shortly after birth, the marginal zone develops into layer I (Boulder Committee, 1970). In neocortex the frequency of Cajal-Retzius neurons has been reported to peak at E13 (König et al., 1977; Raedler and Raedler, 1978), after which their frequencies decline. Functionally, Cajal-Retzius neurons have been thought to play a crucial role in the assistance of radial glia, and they have not been frequently observed in postnatal tissue (Marin-Padilla, 1984). In the present study, Nissl stains suggest that the marginal zone no longer exists by P5. Similar patterns have been observed in the development of visual cortex (Miller, 1981). Cajal-Retzius neurons therefore do not constitute an exception to the inside-out pattern be-

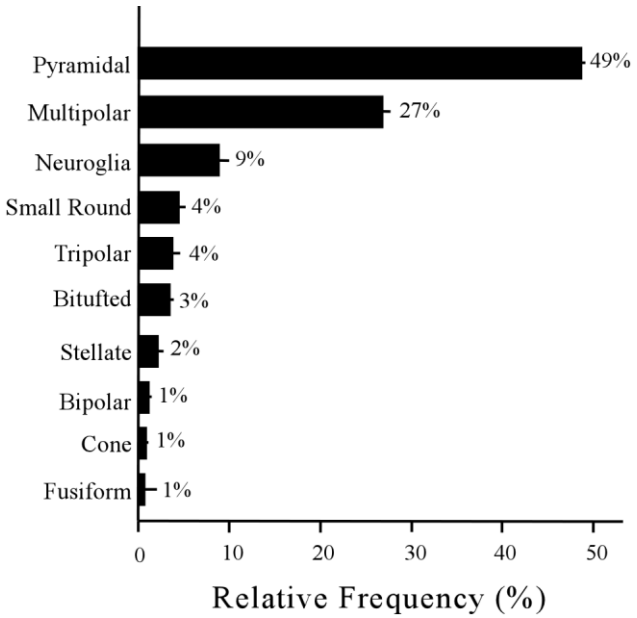

Fig. 13. The relative frequency of Golgi-stained neurons in rat perirhinal cortex as a function of cell type. Data are pooled from eight rats ages P18 through P45 since the distributions do not change after P18. For graphical simplicity, the five subtypes of pyramidal neurons are collapsed into a single group (Pyramidal). For each rat the relative frequency of each individual neuronal class was determined and the data for each of the eight rats were averaged and graphed. Notice that pyramidal and multipolar neurons represent the vast majority (76%) of neurons in perirhinal cortex. Error bars are equal to ± 1 SD.

cause they are better regarded as marginal-zone cells rather than PR layer I neurons.

Large before small neurons. The majority of cells first observed in PR were of the two largest types—pyramidal and multipolar neurons (Fig. 9). The common presumption is that cortical pyramidal and multipolar neurons are excitatory (Peters et al., 1979; Sloper and Powell, 1979; White, 1979; White and Rock, 1980; Schmitt et al., 1981; Peters and Jones, 1984; Kolb and Tees, 1990; Shepard GM, 2004). Smaller, nonpyramidal cell types became more numerous after P6 (Fig. 9). Among the smaller neurons there was no apparent sequencing by size. Small round neurons and aspiny stellate cells, which are presumed to be inhibitory based on their morphology and firing pattern (Faulkner and Brown, 1999; McGann et al., 2001), developed in very different temporal patterns (Fig. 9). The small round neurons, which are readily identifiable in living brain slices (using differential-interference-contrast optics and infrared illumination), invariably have a "fast-firing" spiking pattern (Faulkner and Brown, 1999; McGann et al., 2001).

Stellate neurons were the very last cell class to appear. The postnatal maturation of stellate neurons can therefore be differently affected by ongoing circuit activity. Their late development suggests that this presumed source of inhibitory control of neuronal activity has a delayed onset relative to the formation of much of the rest of the PR circuitry. Note that eye-opening coincides with the increase in the number of stellate neurons (Fig. 9). The first large increase in the number of stellate neurons occurred at P14–17 and the peak was not reached until P28–32. The correspondence of this initial increase in these particular neurons with eye-opening may suggest that the increase could be initiated by sensory-driven input to PR and that the synaptic connections might be shaped by ongoing circuit activity. One suspects that the sequencing and maturation of excitatory and inhibitory cell types may be critical for the functional development of PR, including stability homeostasis (Turrigiano and Nelson, 2004; Padlubnaya et al., 2006).

More persistent dendritic growth in pyramidal neurons. The clear visual impression is that pyramidal cells continue to grow after P18–22 but the nonpyramidal neurons do not. Indeed, 3D reconstructions showed that pyramidal and nonpyramidal neurons have different postnatal growth patterns. After P18–22 there was no detectable increase in the dendritic length in nonpyramidal neurons. By contrast, dendritic length continued to increase (≈2-fold) between P28–32 and P35–40 in pyramidal neurons (Fig. 11A). Greater postnatal dendritic growth in pyramidal than nonpyramidal neurons has also been reported in visual cortex (Uylings et al., 1990, 1994). Due to possible sampling biases resulting from our selection criteria (see Materials and Methods), postnatal dendritic growth in large multipolar neurons may have been underestimated due to growth in the dorsoventral axis. Because the dendrites of these cells are not aligned in any plane, this potential bias is not a consequence of using horizontal sections. Considering the thickness of these tissue sections (200 μm), continued dendritic growth of multipolar neurons should have been detectable after P18–22. Note that dendritic growth in the horizontal plane was easily detected in pyramidal neurons (Fig. 11A). Dendritic length measurements in the small nonpyramidal cells should have been least affected by the selection criteria.

Relative frequency of different cell types

Pyramidal neurons comprised ≈50% of all Golgi-stained cells in PR. Multipolar neurons were the most abundant nonpyramidal cell type (27% of all Golgi-stained cells). The remaining stained neurons in PR consisted of eight morphologically distinct cell types. The relative frequency of nonpyramidal neurons was higher in PR than in any previous description of the rat cerebral cortices to date. In general, pyramidal cells are believed to be the dominant type of cortical neuron (Feldman, 1990) and are frequently reported to comprise ≈70% of the population (Nieuwenhuys, 1994; Valverde, 2002). In visual cortex, where the cellular neuroanatomy has been most thoroughly studied, pyramidal cells constitute as much as 85–95% of the total Golgi-stained neurons (Peters and Kara, 1985, 1987; Peters et al., 1985). Motor cortex, another neocortical region, has been reported to consist of ≈70% pyramidal cells (Winfield et al., 1980). By contrast, only ≈50% of the PR neurons observed here were classified as pyramidal. The percentage of pyramidal cells in layer V of PR (57%) was lower than, but closer to, the percentage of pyramidal cells in layer V of EC (64%; Hamam et al., 2000), which is classified as allocortex. In this respect, PR is structurally more similar to this phylogenetically older region of the cerebral cortex. The larger relative frequency of cell types that are less common in other cortical regions gives the visual impression of greater morphological diversity in PR.

The relative frequency distribution of cell types in layer VI of PR was similar to what has been reported in the basolateral nuclear complex of the amygdala (BLA), in-

cluding the lateral and basolateral nuclei (McDonald, 1982, 1984; Millhouse and DeOlmos, 1983). According to one hypothesis, BLA can be regarded as an extension of the adjacent temporal cortex (McDonald, 1982; Swanson and Petrovich, 1998). McDonald (1982, 1984) found that the most abundant cell type in the BLA was a class I or spiny projection neuron. This classification (McDonald, 1982, 1984) combines characteristics of our multipolar cells and nonupright pyramidal cells. Together these class I or spiny neurons account for ≈70% of cells in the BLA (Millhouse and DeOlmos, 1983). This same classification accounts for ≈60% of cells in layer VI of PR. Although PR shares characteristics with adjacent structures, in terms of the frequencies of cell types within specific layers the overall spatial distribution of cell types is unique to this periallocortical "transition cortex."

Golgi staining versus reconstructions from WCRs

The Golgi method has always furnished the standard for revealing the range of morphological types of neurons that characterize any brain region. The results from the present analysis of 6,891 well-impregnated neurons confirmed several inferences that were previously drawn from a sample of 217 neurons that were labeled during WCRs (Faulkner and Brown, 1999; McGann et al., 2001; Moyer et al., 2002). Both approaches found that roughly half of the cells in layers II/III and V were upright pyramidal cells; that layer I was cell sparse; that layer VI contained mostly nonpyramidal cells and a preponderance of horizontally oriented neurons. Both methods also found a low overall proportion of pyramidal neurons compared with findings from other neocortical areas. Finally, both methods left an overall impression of greater morphological diversity than is typical of other cortices. The Golgi data show that this impression correctly reflects a lower proportion of pyramidal cells and a corresponding increase in the proportion of certain nonpyramidal cell types that occur less frequently in other cortices.

The WCRs suggest that layer V pyramidal neurons might be subject to more refined anatomical classification. These neurophysiological studies suggested that differences in the thickness and rate of taper of the apical dendrite in layer V pyramidal cells are predictive, after a certain age, of whether the neuron spikes in a "burst-firing" mode (versus the more common "regular-firing" mode; Faulkner and Brown, 1999; Moyer et al., 2002). The present study did not attempt to quantify these distinctions among the apical dendrites of layer V pyramidal neurons.

Spatiotemporal patterns of aggregates of neurons

Early in development the Golgi method revealed aggregates of stained neurons (Figs. 5, 7). Aggregates have also been reported during the early development of visual cortex (Miller, 1981). In the present study, aggregates of stained cells were observed in layers I–VI for the first 2 postnatal weeks. After P28, aggregates were observed regularly in layer VI and were sometimes present in deep layer V. It was rare to see aggregates of cells in layer II/III and layer I as age increased. The fact that aggregate frequencies changed in a layer-specific fashion invites speculation. One possibility is that aggregates reflect the manner in which Golgi methods stain electrically coupled neurons. Cortical neurons are often electrically coupled early in development (Naus and Bani-Yaghaoub, 1998). The gap junctions responsible for this intercellular electrical continuity can also pass large dye molecules (Kater and Galvin, 1978; Srinivas et al., 1999; Neijssen et al., 2005).

The ability to exchange molecules enables intercellular chemical communication during early development. Chemical continuity between neurons could conceivably cause the Golgi method to stain electrically coupled groups of neurons. If some of the aggregates result from the manner in which the Golgi methods impregnates electrically coupled neurons, then aggregates in young adulthood could be a sign of electrically coupled cells in deep laminae of PR. In this case, the persistence of cell aggregates may suggest a long-term functional role of gap junctions in deep layer PR neurons, a possibility that can be evaluated using antibodies for connexins that are known to exist in postnatal cortical neurons (Belluardo et al., 2000; Bittman et al., 2002).

SUMMARY AND CONCLUSIONS

Perirhinal cortex is classified as periallocortex (or "transition cortex") because it is phylogenetically intermediate between allocortex and neocortex (Gibb and Kolb, 1998). In terms of neuronal development, PR follows several general laws previously described for neocortex. The visual impression of great morphological heterogeneity among PR neurons reflects the larger relative frequency of cell types that are less common in other cortical regions. The low proportion of pyramidal neurons in PR contrasts with neocortex and is more similar to EC, which is classified as allocortex. The distribution of cell types in the most medial layer of PR (layer VI) is most similar to the adjacent BLA (cf. McDonald, 1982, 1984; Millhouse and DeOlmos, 1983). Although PR shares some characteristics with adjacent structures, the overall cellular morphology and physiology of PR is unique (Faulkner and Brown, 1999; McGann et al., 2001; Moyer et al., 2002).

The conspicuously low myelin content (Zilles and Wree, 1995; Burwell, 2001; Brown and Furtak, 2006) and slow conduction velocity in PR (≈0.2 m/s; Moyer et al., 2002), combined with the slow charging and long-latency firing characteristics of many PR neurons (Moyer and Brown, 1998, 2007; Faulkner and Brown, 1999; Beggs et al., 2000; McGann et al., 2001; Moyer et al., 2002), encourage us to regard this brain region as "slow cortex." This apparent specialization for slow communication possibly offers insight into and seems to place constraints upon the nature of the computations within PR circuits. The intriguing challenge is to understand how the unique cellular morphology and physiology of PR contributes to the manner in which PR circuitry controls the processing, storage, and retrieval of information within the medial temporal lobes. Further understanding of aging-related changes in the relative frequency and laminar distribution of cell types in PR neurons may furnish insight into the selective vulnerability of this brain region to neurodegeneration in Alzheimer's disease.

ACKNOWLEDGMENT

We thank Tyrone Powell for help with cellular reconstructions.

LITERATURE CITED

Allen TA, Furtak SC, Brown TH. 2007. Single-unit responses to 22 kHz ultrasonic vocalizations in rat perirhinal cortex. Behav Brain Res 182: 327–336.

Arnold SE, Hyman BT, Flory J, Damasio AR, Van Hoesen GW. 1991. The topographical and neuroanatomical distribution of neurofibrillary tangles and neuritic plaques in the cerebral cortex of patients with Alzheimer's disease. Cereb Cortex 1:103–116.

Bayer SA, Altman J. 1987. Directions in neurogenetic gradients and patterns of anatomical connections in the telecephalon. Prog Neurobiol 29:57–106.

Beggs JM, Moyer JR, McGann JP, Brown TH. 2000. Prolonged synaptic integration in perirhinal cortical neurons. J Neurophysiol 83:3294–3298.

Belluardo N, Mudò G, Trovato-Salinaro A, Le Gurun S, Charollais A, Serre-Beinier V, Amato G, Haefliger JA, Meda P, Condorelli DF. 2000. Expression of connexin36 in the adult and developing rat brain. Brain Res 865:121–138.

Berry M, Rogers AW. 1965. The migration of neuroblasts in the developing cerebral cortex. J Anat 99:691–709.

Berry M, Rogers AW, Eayrs JT. 1964. Pattern of cell migration during cortical histogenesis. Nature 203:591–593.

Bilkey DK. 1996. Long-term potentiation in the in vitro perirhinal cortex displays associative properties. Brain Res 733:297–300.

Bittman K, Becker DL, Cicirata F, Parnavelas JG. 2002. Connexin expression in homotypic and heterotypic cell coupling in the developing cerebral cortex. J Comp Neurol 443:201–212.

Boulder Committee. 1970. Embryonic vertebrate central nervous system: revised terminology. Anat Rec 166:257–262.

Braak H, Braak E. 1991. Neuropathological stageing of Alzheimer-related changes. Acta Neuropathol 82:239–259.

Braak H, Braak E. 1995. Staging of Alzheimer's disease-related neurofibrillary changes. Neurobiol Aging 16:271–278.

Brown TH, Furtak SC. 2006. Low myelin staining in rat perirhinal cortex and parts of the amygdala. Program No. 638.17. Neuroscience Meeting Planner. Atlanta, GA: Society for Neuroscience, 2006. Online.

Bucci DJ, Phillips RG, Burwell RD. 2000. Contributions of postrhinal and perirhinal cortex to contextual information processing. Behav Neurosci 114:882–894.

Bucci DJ, Saddoris MP, Burwell RD. 2002. Contextual fear discrimination is impaired by damage to the postrhinal or perirhinal cortex. Behav Neurosci 116:479–488.

Buckley MJ, Gaffan D. 1998a. Learning and transfer of object–reward associations and the role of the perirhinal cortex. Behav Neurosci 112:15–23.

Buckley MJ, Gaffan D. 1998b. Perirhinal cortex ablation impairs configural learning and paired-associate learning equally. Neuropsychologia 36:535–546.

Buckley MJ, Booth MCA, Rolls ET, Gaffan D. 2001. Selective perceptual impairments after perirhinal cortex ablation. J Neurosci 21:9824–9836.

Buffalo EA, Reber PJ, Squire LR. 1998. The human perirhinal cortex and recognition memory. Hippocampus 8:330–339.

Burwell RD. 2000. The parahippocampal region: corticocortical connectivity. Ann N Y Acad Sci 911:25–42.

Burwell RD. 2001. Borders and cytoarchitecture of the perirhinal and postrhinal cortices in the rat. J Comp Neurol 437:17–41.

Burwell RD, Amaral DG. 1998a. Perirhinal and postrhinal cortices of the rat: Interconnectivity and connections with the entorhinal cortex. J Comp Neurol 391:293–321.

Burwell RD, Amaral DG. 1998b. Cortical afferents of the perirhinal, postrhinal, and entorhinal cortices of the rat. J Comp Neurol 398:179–205.

Burwell RD, Witter MP, Amaral DG. 1995. Perirhinal and postrhinal cortices of the rat: a review of the neuroanatomical literature and comparison with findings from the monkey brain. Hippocampus 5:390–408.

Bussey TJ, Duck J, Muir JL, Aggleton JP. 2000. Distinct patterns of behavioural impairments resulting from fornix transection or neurotoxic lesions of perirhinal and postrhinal cortices in the rat. Behav Brain Res 111:187–202.

Bussey TJ, Saksida LM, Murray EA. 2002. Perirhinal cortex resolves feature ambiguity in complex visual discriminations. Eur J Neurosci 15:365–374.

Bussey TJ, Saksida LM, Murray EA. 2003. Impairments in visual discrimination after perirhinal cortex lesions: testing 'declarative' vs. 'perceptual-mnemonic' views of perirhinal cortex function. Eur J Neurosci 17:649–660.

Cho K, Aggleton JP, Brown MW, Bashir ZI. 2001. An experimental test of the role of postsynaptic calcium levels in determining synaptic strength using perirhinal cortex of rat. J Physiol 532:459–466.

D'Antuono M, Biagini G, Tancredi V, Avoli M. 2001. Electrophysiology of regular firing cells in the rat perirhinal cortex. Hippocampus 11:662–672.

Eacott MJ, Norman G. 2004. Integrated memory for object, place, and context in rats: a possible model of episodic-like memory? J Neurosci 24:1948–1953.

Faulkner B, Brown TH. 1999. Morphology and physiology of neurons in the rat perirhinal-lateral amygdala area. J Comp Neurol 411:613–642.

Feldman ML. 1990. Morphology of the neocortical pyramidal neuron. In: Kolb B, Tees RC, editors. The cerebral cortex of the rat. Cambridge: MIT Press. p 123–200.

Feldman ML, Peters A. 1978. The forms of non-pyramidal neurons in the visual cortex of the rat. J Comp Neurol 179:761–794.

Furtak SC, Wei S-M, Agster KL, Burwell RD. 2007. Functional neuroanatomy of the parahippocampal region in the rat: the perirhinal and postrhinal cortices. Hippocampus (in press).

Gibb R, Kolb B. 1998. A method for vibratome sectioning of Golgi-Cox stained whole rat brain. J Neurosci Methods 79:1–4.

Hamam BN, Kennedy TE, Alonso A, Amaral DG. 2000. Morphological and electrophysiological characteristics of layer V neurons of the rat medial entorhinal cortex. J Comp Neurol 418:457–472.

Hannesson DK, Howland JG, Phillips AG. 2004. Interaction between perirhinal and medial prefrontal cortex is required for temporal order but not recognition memory for objects in rats. J Neurosci 24:4596–4604.

Hicks SP, D'Amato CJ. 1968. Cell migrations to the isocrotex in the rat. Anat Rec 160:619–634.

Holdstock JS, Gutnikov SA, Gaffan D, Mayes AR. 2000. Perceptual and mnemonic matching-to-sample in humans: contributions of the hippocampus, perirhinal and other medial temporal lobe cortices. Cortex 36:301.322.

Jacobson M. 1991. Developmental neurobiology, 3rd ed. New York: Plenum Press.

Jones EG. 1984. Neurogliaform or spiderweb cells. In: Peters A, Jones EG, editors. Cerebral cortex, vol 1. Cellular components of the cerebral cortex. New York: Plenum Press. p 409–418.

Juottonen K, Laakso MP, Insausti R, Lehtovirta M, Pitkänen A, Partanen K, Soininen H. 1998. Volumes of the entorhinal and perirhinal cortices in Alzheimer's disease. Neurobiol Aging 19:15–22.

Kater SB, Galvin NJ. 1978. Physiological and morphological evidence for coupling in mouse salivary gland acinar cells. J Cell Biol 79:20–26.

Kolb B, Tees RC (Eds.). 1990. The cerebral cortex of the rat. Cambridge: MIT Press.

König N, Valat J, Fulcrand J, Marty R. 1977. The time of origin of Cajal-Retzius cells in the rat temporal cortex. An autoradiographic study. Neurosci Lett 4:21–26.

Lee AC, Bussey TJ, Murray EA, Saksida LM, Epstein RA, Kapur N, Hodges JR, Graham KS. 2005. Perceptual deficits in amnesia: challenging the medial temporal lobe 'mnemonic' view. Neuropsychologia 43:1–11.

Levy DA, Bayley PJ, Squire LR. 2004. The anatomy of semantic knowledge: Medial vs lateral temporal lobe. Proc Natl Acad Sci U S A 101:6710–6715.

Lindquist DH, Jarrard LE, Brown TH. 2004. Perirhinal cortex supports delay fear conditioning to rat ultrasonic social signals. J Neurosci 24:3610–3617.

Liu P, Bilkey DK. 1996. Long-term potentiation in the perirhinal-hippocampal pathway is NMDA dependent. Neuroreport 7:1241–1244.

Liu P, Bilkey DK. 1998. Excitotoxic lesions centered on perirhinal cortex produce delay-dependent deficits in a test of spatial memory. Behav Neurosci 112:512–524.

Liu P, Bilkey DK. 2001. The effects of excitotoxic lesions centered on the hippocampus or perirhinal cortex in object recognition and spatial memory tasks. Behav Neurosci 115:94–111.

Lorente de No R. 1933. Studies on the structure of the cerebral cortex. J Psychol Neurol 45:381–438.

Lorente de No R. 1934. Studies on the structure of the cerebral cortex. II. Continuation of the study of the Ammonic system. J Psychol Neurol 46:113–177.

Marin-Padilla M. 1984. Neurons of layer I: a developmental analysis. In:

Peters A, Jones EG, editors. Cerebral cortex, vol. 1. Cellular components of the cerebral cortex. New York: Plenum Press. p 447–478

McDonald AJ. 1982. Neurons of the lateral and basolateral amygdaloid nuclei: a Golgi study in the rat. J Comp Neurol 212:293–312.

McDonald AJ. 1984. Neuronal organization of the lateral and basolateral amygdaloid nuclei in the rat. J Comp Neurol 222:589–606.

McGann JP, Moyer JR Jr, Brown TH. 2001. Predominance of late-spiking neurons in layer VI of rat perirhinal cortex. J Neurosci21:4969–4976.

Meunier M, Bachevalier J, Mishkin M, Murray EA. 1993. Effects on visual recognition of combined and separate ablations of the entorhinal and perirhinal cortex in rhesus monkeys. J Neurosci 13:5418–5432.

Miller M. 1981. Maturation of the rat visual cortex. I. A quantitative study of Golgi-impregnated pyramidal neurons. J Neurocytol 10:859–878.

Millhouse OE, DeOlmos J. 1983. Neuronal configurations in lateral and basolateral amygdala. Neuroscience 10:1269–1300.

Moyer JR Jr, Brown TH. 1998. Methods for whole-cell recording from visually preselected neurons of perirhinal cortex in brain slices from young and aging rats. J Neurosci Methods 86:35–54.

Moyer JR Jr, Brown TH. 2007. Visually guided patch-clamp recordings in brain slices. In: Walz W, editor. Patch-clamp analysis: advanced techniques for patch-clamp analysis, 3rd ed. Totowa, NJ: Humana Press. p 169–228.

Moyer JR Jr, McNay EC, Brown TH. 2002. Three classes of pyramidal cells in layer V of rat perirhinal cortex. Hippocampus 12:218–234.

Naber PA, Witter MP, Lopes da Silva FH. 1999. Perirhinal cortex input to the hippocampus in the rat: evidence for parallel pathways, both direct and indirect. A combined physiological and anatomical study. Eur J Neurosci 11:4119–4133.

Naus CCG, Bani-Yaghoub M. 1998. Gap junctional communication in the developing central nervous system. Cell Biol Int 22:751–763.

Neijssen J, Herberts C, Drijfhout JW, Reits E, Janssen L, Neefjes J. 2005. Cross-presentation by intercellular peptide transfer through gap junctions. Nature 434:83–88.

Nieuwenhuys R. 1994. The neocortex. An overview of its evolutionary development, structural organization and synaptology. Anat Embryol 190:307–337.

Norman G, Eacott MJ. 2004. Impaired object recognition with increasing levels of feature ambiguity in rats with perirhinal cortex lesions. Behav Brain Res 148:79–91.

Padlubnaya DB, Parekh NH, Brown TH. 2006. Neurophysiological theory of Kamin blocking in fear conditioning. Behav Neurosci 120:337–352.

Pasternak JF, Woolsey TA. 1975. On the "selectivity" of the Golgi-Cox method. J Comp Neurol 160:307–312.

Paxinos G, Watson C. 1998. The rat brain in stereotaxic coordinates. San Diego: Academic Press.

Peters A. 1984. Bipolar Cells. In: Peters A, Jones EG, editors. Cerebral cortex, vol. 1. Cellular components of the cerebral cortex. New York: Plenum Press. p 381–408.

Peters A, Jones EG (Eds.). 1984. Cerebral cortex, vol. 1. New York: Plenum Press.

Peters A, Kara DA. 1985. The neuronal composition of area 17 of rat visual cortex. I. The pyramidal cells. J Comp Neurol 234:218–241.

Peters A, Kara DA. 1987. The neuronal composition of area 17 of rat visual cortex. IV. The organization of pyramidal cells. J Comp Neurol 260: 573–590.

Peters A, Regidor J. 1981. A reassessment of the forms of nonpyramidal neurons in area 17 of cat visual cortex. J Comp Neurol 203:685–716.

Peters A, Proskauer CC, Feldman MC, Kimerer L. 1979. The projections of the lateral geniculate nucleus to area 17 of the rat cerebral cortex. V. Degenerating axon terminals synapsing with Golgi-impregnated neurons. J Neurocytol 8:331–357.

Peters A, Kara DA, Harriman KM. 1985. The neuronal composition of area 17 of rat visual cortex. III. Numerical considerations. J Comp Neurol 238:263–274.

Pikkarainen M, Pitkänen A. 2001. Projections from the lateral, basal and accessory basal nuclei of the amygdala to the perirhinal and postrhinal cortices in the rat. Cereb Cortex 11:1064–1082.

Pitkänen A, Pikkarainen M, Nurminen N, Ylinen A. 2000. Reciprocal connections between the amygdala and the hippocampal formation, perirhinal cortex, and postrhinal cortex in rat. Ann N Y Acad Sci 911:369–391.

Price DJ, Willshaw DJ. 2000. Mechanisms of cortical development. New York: Oxford University Press.

Raedler E, Raedler A. 1978. Autoradiographic study of early neurogenesis in rat neocortex. Anat Embryol 154:267–284.

Ramón y Cajal S. 1911. Histology of the nervous system. Swanson N, Swanson L, translators. New York: Oxford University Press.

Romanski LM, LeDoux JE. 1993. Information casade from primary auditory cortex to the amygdala: corticocortical and corticoamygdaloid projections of temporal cortex in the rat. Cereb Cortex 3:515–532.

Schmitt FO, Worden FG, Adelman G, Dennis SG (Eds.). 1981. The organization of the cerebral cortex: proceedings of a neuroscience research colloquium. Cambridge: MIT Press.

Scoville WB, Milner B. 1957. Loss of recent memory after bilateral hippocampal lesions. J Neurol Neurosurg Psychiatry 20:11–21.

Shepard GM. 2004. The synaptic organization of the brain, 5th ed. New York: Oxford University Press.

Shi CJ, Cassell MD. 1999. Perirhinal cortex projections to the amygdaloid complex and hippocampal formation in the rat. J Comp Neurol 406: 299–328.

Sloper JJ, Powell TPS. 1979. An experimental electron microscopic study of afferent connections to the primate motor and somatic sensory cortices. Philos Trans R Soc Lond B 285:199–226.

Smit GJ, Colon EJ. 1969. Quantitative analysis of the cerebral cortex. I. Aselectivity of the Golgi-Cox staining technique. Brain Res 13:485–510.

Srinivas M, Rozental R, Kojima T, Dermietzel R, Mehler M, Condorelli DF, Kessler JA, Spray DC. 1999. Functional properties of channels formed by the neuronal gap junction protein connexin36. J Neurosci 19:9848–9855.

Suzuki WA, Zola-Morgan S, Squire LR, Amaral DG. 1993. Lesions of the perirhinal and parahippocampal cortices in the monkey produce long-lasting memory impairment in the visual and tactual modalities. J Neurosci 13:2430–2451.

Swanson LW, Petrovich GD. What is the amygdala? Trends Neurosci 21:323–331.

Turrigiano GG, Nelson SB. 2004. Homeostatic plasticity in the developing nervous system. Nat Rev Neurosci 5:97–107.

Uylings HBM. 2000. Development of the cerebral cortex in rodents and man. Eur J Morphol 38:309–312.

Uylings HBM, Van Eden CG, Parnavelas JG, Kalsbeek A. 1990. The prenatal and postnatal development of rat cerebral cortex. In: Kolb B, Tees RC, eds. The cerebral cortex of the rat. Cambridge, MA: MIT Press. p 35–76.

Uylings HBM, van Pelt J, Parnavelas JG, Ruiz-Marcos A. 1994. Geometrical and topological characteristics in the dendritic development of cortical pyramidal and non-pyramidal neurons. Prog Brain Res 102: 109–123.

Valverde F. 2002. Structure of the cerebral cortex. Intrinsic organization and comparative analysis of the neocortex. Rev Neurol 34:758–780.

Van Hoesen GW, Solodkin A. 1994. Cellular and systems neuroanatomical changes in Alzheimer's disease. Ann N Y Acad Sci 747:12–35.

Van Hoesen GW, Augustinack JC, Dierking J, Redman SJ, Thangavel R. 2000. The parahippocampal gyrus in Alzheimer's disease: clinical and preclinical neuroanatomical correlates. Ann N Y Acad Sci 911: 254–274.

White EL. 1979. Thalamocortical synaptic relations: a review with emphasis on the projections of specific thalamic nuclei to the primary sensory areas of the neocortex. Brain Res Rev 1:275–311.

White EL, Rock MP. 1980. Three-dimensional aspects and synaptic relationships of a Golgi-impregnated spiny stellate cell reconstructed from serial thin sections. J Neurocytol 9:615–636.

Winfield DA, Gatter KC, Powell TPS. 1980. An electron microscopic study of the types and proportions of neurons in the cortex of the motor and visual areas of the cat and rat. Brain 103:245–258.

Zilles K, Wree A. 1995. Cortex: areal and laminar structure. In: Paxinos G, ed. The rat nervous system. San Diego: Academic Press. p 649–685.

Zola-Morgan S, Squire LR, Amaral DG, Suzuki WA. 1989. Lesions of perirhinal and parahippocampal cortex that spare the amygdala and hippocampal formation produce severe memory impairment. J Neurosci 9:4355–4370.

Zola-Morgan S, Squire L, Clower R, Rempel NL. 1993. Damage to the perirhinal cortex exacerbates memory impairment following lesions to the hippocampal formation. J Neurosci 13:251–265.